https://ntrs.nasa.gov/search.jsp?R=19930088903 2020-06-17T08:59:18+00:00Z



NACA RM L55I16

NACA

# RESEARCH MEMORANDUM

## THE EFFECT OF LEADING-EDGE DROOP UPON THE PRESSURE DISTRIBUTION AND AERODYNAMIC LOADING CHARACTERISTICS OF A 45° SWEPTBACK WING AT TRANSONIC SPEEDS

By James W. Schmeer

Langley Aeronautical Laboratory
Langley Field, Va.

NATIONAL ADVISORY COMMITTEE FOR AERONAUTICS

WASHINGTON

November 8, 1955
Declassified September 13, 1957

NACA RM L55I16

NATIONAL ADVISORY COMMITTEE FOR AERONAUTICS

---

RESEARCH MEMORANDUM

---

# THE EFFECT OF LEADING-EDGE DROOP UPON THE PRESSURE DISTRIBUTION AND AERODYNAMIC LOADING CHARACTERISTICS OF A 45° SWEPTBACK WING AT TRANSONIC SPEEDS

By James W. Schmeer

## SUMMARY

An investigation was conducted in the Langley 16-foot transonic tunnel to determine the effects of leading-edge droop on the pressure distribution on a 45° sweptback wing with an aspect ratio of 4, a taper ratio of 0.6, and NACA 65A006 airfoil sections parallel to the plane of symmetry. The leading edge of the wing was drooped 6° about the 19-percent chord line from 0.15 semispan to the wing tip. Data were obtained at Mach numbers of 0.80 to 1.03 with average Reynolds numbers of $5.7 \times 10^6$ to $6.3 \times 10^6$, respectively. The results of this investigation are compared with the pressure data obtained with the undrooped or basic wing of a previous investigation.

The comparisons indicated that leading-edge droop delayed separation on the outboard sections of the wing to higher angles of attack for Mach numbers up to about 0.94. At this Mach number and higher, shock waves are the predominant phenomena on the upper surface of the wing; no significant benefits were derived from the drooped leading edge in this speed range. The center of pressure was shifted rearward about 12 to 15 percent at low normal-force coefficients for all Mach numbers; at higher normal-force coefficients, the effect of leading-edge droop was generally decreased. The maximum difference in lateral-center-of-pressure location was about a 7.5-percent outboard shift due to leading-edge droop. This difference occurred at the lower Mach numbers at moderate normal-force coefficients where leading-edge droop delayed tip separation. At these conditions, the wing-root bending moments would be higher for the wing with drooped leading edge as compared with those for the basic wing.

## INTRODUCTION

Several investigations have indicated the effects of leading-edge droop on the force and moment characteristics of thin swept wings at high subsonic and transonic speeds (refs. 1 to 3). However, little or no information is currently available concerning the effects of leading-edge droop on the pressure distributions and aerodynamic loading characteristics of wings operating in this speed range. The present investigation was, therefore, conducted in the Langley 16-foot transonic tunnel in order to obtain pressure data, aerodynamic loading and associated flow phenomena for a typical swept wing with leading-edge droop.

The wing used in this investigation had 45° sweepback of the quarter-chord line, a taper ratio of 0.6, an aspect ratio of 4, and basic NACA 65A006 airfoil sections parallel to the plane of symmetry. The leading edge of the wing was drooped 6° about the 19-percent chord line from 0.15 semispan to the wing tip.

Pressure data were obtained through an angle-of-attack range of 0° to about 20° at Mach numbers of 0.80 to 0.94, and of 0° to about 12° at Mach numbers of 0.98 to 1.03. The results are compared herein with the pressure data for the undrooped or basic wing which was reported in reference 4. Ink-flow pictures are also included to aid in visualizing the flow phenomena on the upper surface of the wing with leading-edge droop. Force and moment data for the configuration with leading-edge droop obtained simultaneously with the pressure data, have been presented in reference 5.

## SYMBOLS

| | |
|---|---|
| $b$ | wing span |
| $c$ | local wing chord |
| $c'$ | wing mean aerodynamic chord |
| $\bar{c}$ | average wing chord |
| $c_m \frac{c^2}{\bar{c}c'}$ | wing-section pitching-moment parameter with moment about $c'/4$, $\frac{c^2}{\bar{c}c'} \int_0^1 \left(P_L - P_U\right)\left(\frac{x_1}{c} - \frac{x}{c}\right) d\frac{x}{c}$ |

$C_{m_{c'/4}}$ wing-panel pitching-moment coefficient, $\int_{0.135}^{1.0} \left(c_m \frac{c^2}{\bar{c}c'}\right) d\frac{y}{b/2}$

$c_n \frac{c}{\bar{c}}$ wing-section normal-load parameter, $\frac{c}{\bar{c}} \int_0^1 (P_L - P_U) d\frac{x}{c}$

$c_n'$ wing-section normal-force coefficient for the forward 19 percent of the wing, $\int_0^{.19} (P_L - P_U) d\frac{x}{c}$

$C_N$ wing-panel normal-force coefficient, $\int_{0.135}^{1.0} c_n \frac{c}{\bar{c}} d\frac{y}{b/2}$

$C_{N'}$ normal-force coefficient for the forward 19 percent of the wing panel, $\int_{0.135}^{1.0} c_n' \frac{c}{\bar{c}} d\frac{y}{b/2}$

M free-stream Mach number

P pressure coefficient, $\frac{p - p_\infty}{q}$

p local static pressure

$p_\infty$ free-stream static pressure

q free-stream dynamic pressure

x distance from wing leading edge at a given spanwise station, positive downstream

$x_1$ distance from wing leading edge at a given spanwise station to line perpendicular to plane of symmetry and passing through c'/4, positive downstream

$x_{cp/c}$ longitudinal location of wing-section center of pressure,

$$0.25 - \int_0^1 \frac{\left(P_L - P_U\right)\left(0.25 - \frac{x}{c}\right) d\,\frac{x}{c}}{c_n}$$

$X_{cp/c'}$ longitudinal location of wing-panel center of pressure,

$$0.25 - \frac{C_{m_{c'}}/4}{C_N}$$

$y$ spanwise distance from the plane of symmetry

$Y_{cp/b/2}$ lateral location of wing-panel center of pressure,

$$\int_{0.135}^{1.0} \frac{\left(c_n \frac{c}{\bar{c}}\right)\left(\frac{y}{b/2}\right) d\,\frac{y}{b/2}}{C_N}$$

$\alpha$ angle of attack of fuselage center line

Subscripts:

L lower surface of wing

U upper surface of wing

## APPARATUS AND TESTS

### Tunnel

The investigation was made in the Langley 16-foot transonic tunnel, which is described in reference 6.

### Model

The fuselage and wings were constructed of magnesium and steel, respectively. For this investigation, the basic wing used in reference 4 was cut at the 19-percent chord line from 0.15 semispan to the wing tip and the leading edge was drooped 6° about this line. A photograph of the model mounted in the test section of the 16-foot transonic tunnel is presented in figure 1; a sketch showing the important model dimensions and wing data is presented in figure 2. The pressure-orifice distribution on the upper and lower surface of the wing is identical.

### Tests

Pressure measurements were obtained through an angle-of-attack range of 0° to about 20° at Mach numbers of 0.80 to 0.94 and from 0° to about 12° at Mach numbers of 0.98 to 1.03. The average Reynolds number based on the mean aerodynamic chord varied from $5.7 \times 10^6$ at a Mach number of 0.80 to $6.3 \times 10^6$ at a Mach number of 1.03. The basic-wing data presented herein were previously published in reference 4.

Ink-flow tests were made at a constant Mach number while the angle of attack was increasing at a steady rate of about 4° per minute. A mixture of Prussian blue and an organic solvent was continuously emitted from eight orifices distributed across the semispan as shown in figure 2 and still pictures were taken at about every half degree; motion pictures were also taken through the complete angle-of-attack range. Further details on the ink-flow technique can be found in reference 7.

## RESULTS AND DISCUSSION

The results of this investigation are presented in figures 3 to 11 which also include for comparison some of the basic-wing data published in reference 4. Comparisons of the pressure-coefficient distributions at selected angles of attack are presented in figure 3. The wing-panel characteristics presented in figures 4 to 6 and the section characteristics in figures 7 and 8 were obtained by integration of the wing pressures as indicated in the list of symbols. Some additional loading data for the wing leading edge are shown in figures 9 and 10. Finally, ink-flow pictures illustrating the flow over the surface of the wing with 6° leading-edge droop are presented in figure 11. Because detailed studies of the flow phenomena and loading characteristics of the basic wing have previously been published (see refs. 8 to 11), the following discussion will be limited to the significant differences attributable to the drooped leading edge.

### Chordwise Pressure Distributions

In figure 3, comparisons of the pressure-coefficient distributions for the basic wing and the wing with drooped leading edge are presented at seven spanwise stations. Generally, the flow phenomena for the two wings are quite similar, with the main differences occurring, of course, on the drooped part of the wing. Furthermore, the beneficial effects that were derived from the drooped leading edge, were usually confined to the outboard sections of the wing.

The curves for zero angle of attack in figure 3 show that at all test Mach numbers the pressures on the two wings assumed nearly identical values beginning a short distance rearward of the drooped-leading-edge hinge line ($x/c = 0.19$).

With an increase in angle of attack to 4° at a Mach number of 0.80 (fig. 3(a)), a negative pressure spike, indicating a high local velocity, appears along the 20-percent-chord line of the wing with leading-edge droop. As at zero angle of attack, the pressures behind this line are nearly the same for both wings. However, with increasing Mach number (figs. 3(b) to 3(f)), this negative pressure peak becomes flat and broader in width. The chordwise extent of this area of relatively high supersonic flow increases toward the wing tip at the higher Mach numbers and seems to be defined by one or more of the several shock waves present (depending on spanwise station and free-stream Mach number). For a typical example, see figure 3(c), showing the pressure distribution at a Mach number of 0.94 and 4° angle of attack. Here, with the aid of the ink-flow picture for the same condition (fig. 11(c)), the following observations of the flow can be made. A shock wave originating near the junction of the fuselage and the hinge line of the drooped leading edge sweeps across the wing panel as indicated by the kinks in the streamwise flow of ink. At semispan stations of 0.25 and 0.40, this shock wave is just behind the hinge line of the drooped leading edge and sharp pressure peaks (due to expansion about the bend in the upper surface) occur at these stations. At progressively more outboard stations to about $2y/b = 0.85$, the shock wave sweeps further aft of the hinge line and, therefore, allows the pressure peak to spread rearward. Slightly outboard of semispan station $2y/b = 0.85$, the shock wave associated with the fuselage-hinge line juncture merges with a combination of the trailing-edge shock and the main-flow deceleration shock. These three combined shock waves occur farther forward on the wing near the tip and thus the chordwise extent of the high-velocity flow at semispan station 0.95 is somewhat reduced.

With an increase in angle of attack to 8° at a Mach number of 0.80 (fig. 3(a)), the drooped leading edge delays separation on the outboard sections of the wing, maintains higher leading-edge suction, and thereby reduces drag as indicated in reference 5. However, with increasing Mach number, this beneficial effect of higher leading-edge suction diminishes and disappears before a Mach number of 0.98 is attained. At a Mach number of about 0.94 and above, the predominant difference between the flow over the two wings is the flat pressure distribution between the hinge line of the drooped leading edge and the shock waves, as discussed for 4° angle of attack. Here, again, the ink-flow pictures of figure 11 can be useful in visualizing the flow phenomena.

At the higher angles of attack, there is no direct comparison of pressure distributions at equal angles; however, the effects of leading-edge droop are indicated. Figure 3(a) shows that at a Mach number of 0.80 severe separation exists on the outboard 50 percent of the basic wing at 11.2°, whereas, the wing with the drooped leading edge, except for some separation at the tip, maintains a well distributed load up to 12.5°. However, with an increase in Mach number to 0.90 and 0.94 (figs. 3(b) and 3(c)) the outboard sections of the wing with droop show extensive

separation and the distributions for the two wings are, for all practical purposes, identical. At these two Mach numbers, the leading-edge droop provides small increases in pressure coefficients over the midsemispan sections. At higher Mach numbers, where shock waves are the predominant phenomena on the upper surface of the wing, leading-edge droop loses its effectiveness. Moreover, at the highest angles of attack, severe separation occurs on the upper surface of both wings and the pressure distributions become essentially the same.

## Wing-Panel Characteristics

Normal force and pitching moments.- The effect of $6^\circ$ leading-edge droop on the wing normal force is shown in figure 4. An increase in $C_N$ of about 0.1 is obtained at a Mach number of 0.80 and angle of attack of $12^\circ$. This gain in normal-force coefficient decreases both with increasing angle of attack and Mach number, with no gain realized at a Mach number of 1.00 or 1.03 within the angle-of-attack range of these tests.

The pitching-moment curves of figure 5 show that the wing with leading-edge droop had more negative values of pitching-moment coefficient at all Mach numbers. Also, wherever the angle of attack was high enough to cause an unstable break in the pitching-moment curves, the leading-edge droop delayed the break to somewhat higher values of normal-force coefficient. However, the severity of the break was greater.

Center of pressure.- The center of pressure for the wing with leading-edge droop was shifted rearward about 12 to 15 percent (as compared to the basic wing) at low normal-force coefficients for all Mach numbers (fig. 6(a)). This difference generally decreased with increasing $C_N$ as the drooped leading edge assumed a greater portion of the normal load.

The largest difference in lateral center-of-pressure location (about 7.5 percent of the semispan) occurred at a Mach number of 0.80 at a normal-force coefficient of approximately 0.65 (fig. 6(b)). In this speed range (up to a Mach number of about 0.94) leading-edge droop delayed the inboard shift of center of pressure which is characteristic of swept wings at moderate angles of attack. The more outboard position of the center of pressure results, of course, in higher bending moments for the wing with leading-edge droop.

## Wing-Section Characteristics

Spanwise loading distribution.- Comparisons of the normal-load parameter, $c_n \frac{c}{\bar{c}}$, are shown at several angles of attack in figure 7. In

general, the effects of leading-edge droop are similar for all the test Mach numbers at low angles of attack where the basic wing, as expected, carries more load across the entire span. With increasing angle of attack at Mach numbers up to about 0.94 the leading-edge droop delays the loss in normal load which starts at the wing tip and progresses inboard (span loading changes from elliptical to roughly triangular). However, at the higher Mach numbers leading-edge droop provided little or no improvement over the basic wing which maintained tip loads to the highest angle tested. At all Mach numbers above 0.80, leading-edge droop reduced the normal load on the inboard sections out to about the 40-percent semispan station.

Section center of pressure.- The effect of leading-edge droop on the wing-section centers of pressure is shown in figure 8. Generally, the trends with angle of attack for each section are very similar to that for the complete panel previously discussed.

## Maximum Additional Normal Load on Wing Leading Edge

The data of these tests indicated that the maximum increase in normal loading due to leading-edge droop occurred at a Mach number of 0.80 and diminished with increasing speed; the same trend was true for the droopable leading edge alone as well as for the complete wing panel. The section normal-force coefficient $c_n'$ for the leading edge of the wing, shown for two semispan stations and two Mach numbers in figure 9, illustrates this point. The maximum additional loading on the leading edge itself, therefore, is indicated in figure 10 where the normal-force coefficient $C_N'$ is plotted against angle of attack at a Mach number of 0.80. This figure shows an increase in $C_N'$ of 0.05 (about 23 percent) due to 6° deflection, with the maximum load occurring at 10° angle of attack for the undeflected leading edge and 12.5° for the 6° deflected leading edge.

## CONCLUSIONS

The results of an investigation of the effects of leading-edge droop on the pressure distribution and loading characteristics of a 45° swept-back wing with an aspect ratio of 4, a taper ratio of 0.6, and NACA 65A006 airfoil sections parallel to the plane of symmetry lead to the following conclusions:

1. Leading-edge droop delayed the onset of separation on the outboard sections of the wing at a Mach number of 0.80; this beneficial effect diminished with speed. At a Mach number of about 0.94 and higher, shock waves are the predominant phenomena on the upper surface of the wing;

no significant benefits were derived from the drooped leading edge in this speed range.

2. Leading-edge droop shifted the center of pressure rearward 12 to 15 percent for all the test Mach numbers at low normal-force coefficients. At higher normal-force coefficients, this rearward shift generally decreased.

3. Leading-edge droop delayed the inboard shift of center of pressure so that there was a maximum difference in lateral location of about 7.5 percent of the semispan. This delay, occurring at moderate normal-force coefficients at Mach numbers of 0.80 to 0.94, results in greater wing-root bending moments for the wing with leading-edge droop.

Langley Aeronautical Laboratory,
National Advisory Committee for Aeronautics,
Langley Field, Va., August 31, 1955.

## REFERENCES

1. Spreeman, Kenneth P., and Alford, William J., Jr.: Investigation of the Effects of Leading-Edge Flaps on the Aerodynamic Characteristics in Pitch at Mach Numbers From 0.40 to 0.93 of a Wing-Fuselage Configuration With a 45° Sweptback Wing of Aspect Ratio 4. NACA RM L53G13, 1953.

2. Spreeman, Kenneth P., and Alford, William J., Jr.: Small-Scale Transonic Investigation of the Effects of Full-Span and Partial-Span Leading-Edge Flaps on the Aerodynamic Characteristics of a 50° 38' Sweptback Wing of Aspect Ratio 2.98. NACA RM L52E12, 1952.

3. Hieser, Gerald: An Investigation at Transonic Speeds of the Effects of Fences, Drooped Nose, and Vortex Generators on the Aerodynamic Characteristics of a Wing-Fuselage Combination Having a 6-Percent-Thick, 45° Sweptback Wing. NACA RM L53B04, 1953.

4. Hallissy, Joseph M., Jr., West, F. E., Jr., and Liner, George: Effects of Spoiler Ailerons on the Aerodynamic Load Distribution Over a 45° Sweptback Wing at Mach Numbers From 0.60 to 1.03. NACA RM L54C17a, 1954.

5. Schmeer, James W., and Cooper, J. Lawrence: Effects of Increasing Reynolds Number From $2 \times 10^6$ to $6 \times 10^6$ on the Aerodynamic Characteristics at Transonic Speeds of a 45° Swept Wing With 6° Leading-Edge Droop. NACA RM L54L10, 1954.

6. Ward, Vernon G., Whitcomb, Charles F., and Pearson, Merwin D.: Air-Flow and Power Characteristics of the Langley 16-Foot Transonic Wind Tunnel With Slotted Test Section. NACA RM L52E01, 1952.

7. Runckel, Jack F., and Schmeer, James W.: The Aerodynamic Characteristics at Transonic Speeds of a Model With a 45° Sweptback Wing, Including the Effect of Leading-Edge Slats and a Low Horizontal Tail. NACA RM L53J08, 1954.

8. Whitcomb, Richard T., and Kelly, Thomas C.: A Study of the Flow Over a 45° Sweptback Wing-Fuselage Combination at Transonic Mach Numbers. NACA RM L52D01, 1952.

9. Loving, Donald L., and Williams, Claude V.: Aerodynamic Loading Characteristics of a Wing-Fuselage Combination Having a Wing of 45° Sweepback Measured in the Langley 8-Foot Transonic Tunnel. NACA RM L52B27, 1952.

10. Solomon, William, and Schmeer, James W.: Effect of Longitudinal Wing Position on the Pressure Characteristics at Transonic Speeds of a 45° Sweptback Wing-Fuselage Model. NACA RM L52K05a, 1953.

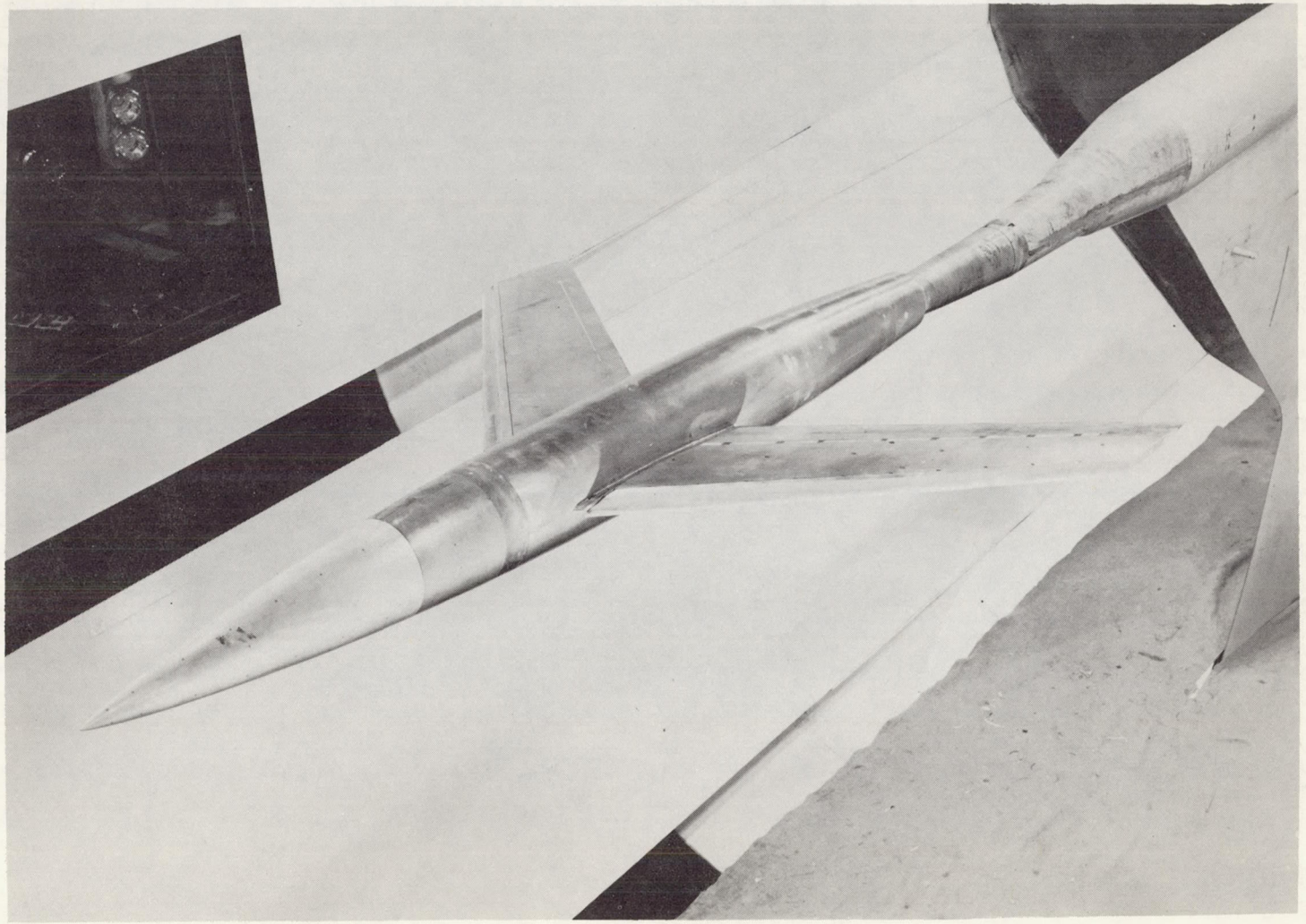

L-82931.1

Figure 1.- The model in the Langley 16-foot transonic tunnel. The wings have 6° leading-edge droop.

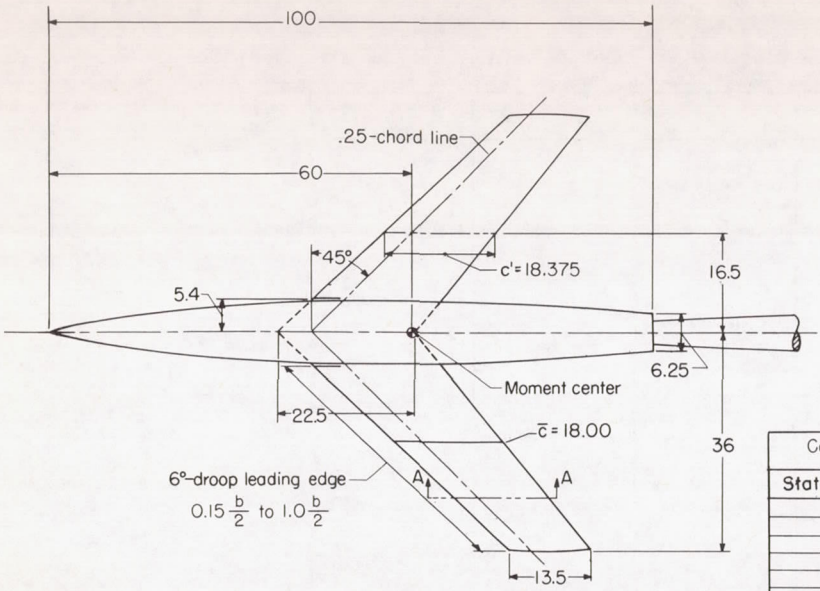


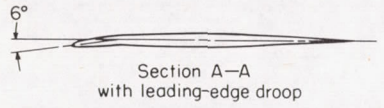


Wing orifice location at each of seven stations

Percent chord

| | |
|---|---|
| 0 | 45.00 |
| 1.25 | 50.00 |
| 2.50 | 55.00 |
| 5.00 | 60.00 |
| 7.50 | 65.00 |
| 10.00 | 70.00 |
| 15.00 | 75.00 |
| 20.00 | 80.00 |
| 25.00 | 85.00 |
| 30.00 | 90.00 |
| 35.00 | 95.00 |
| 40.00 | |

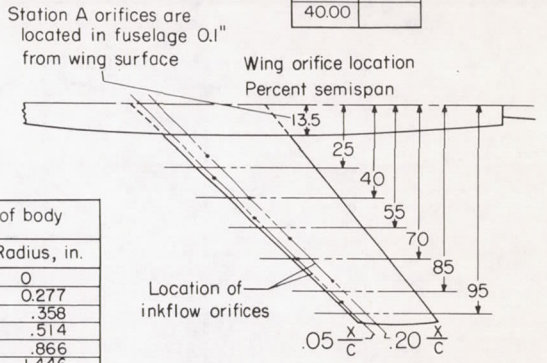


| Coordinates of body | |
|---|---|
| Station, in. | Radius, in. |
| 0 | 0 |
| 0.6 | 0.277 |
| .9 | .358 |
| 1.5 | .514 |
| 3.0 | .866 |
| 6.0 | 1.446 |
| 9.0 | 1.936 |
| 12.0 | 2.365 |
| 18.0 | 3.112 |
| 24.0 | 3.708 |
| 30.0 | 4.158 |
| 36.0 | 4.489 |
| 42.0 | 4.719 |
| 48.0 | 4.896 |
| 54.0 | 4.971 |
| 60.0 | 5.000 |
| 66.0 | 4.955 |
| 72.0 | 4.830 |
| 78.0 | 4.580 |
| 84.0 | 4.245 |
| 90.0 | 3.853 |
| 96.0 | 3.420 |
| 100.0 | 3.125 |
| Nose radius | .060 |

| Wing data | |
|---|---|
| Taper ratio | 0.6 |
| Aspect ratio | 4.0 |
| Wing area | 9 sq. ft. |
| Airfoil section | NACA 65A006 parallel to plane of symmetry |

Figure 2.- Diagram of the wing-fuselage model showing the dimensional details and the location of the pressure orifices. All linear dimensions are in inches.

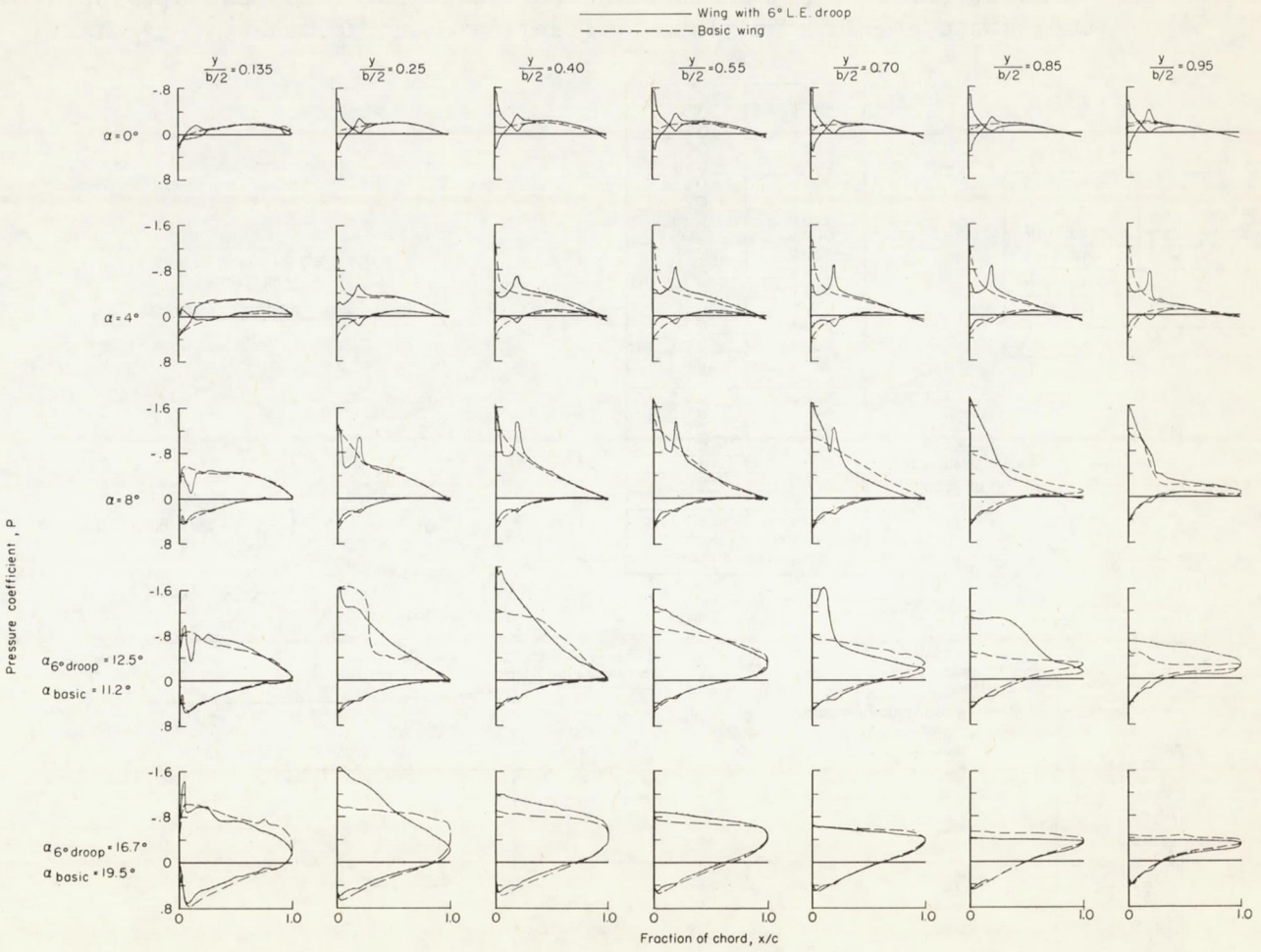


(a) M = 0.80.

Figure 3.- Chordwise pressure distributions for the wing with and without leading-edge droop.

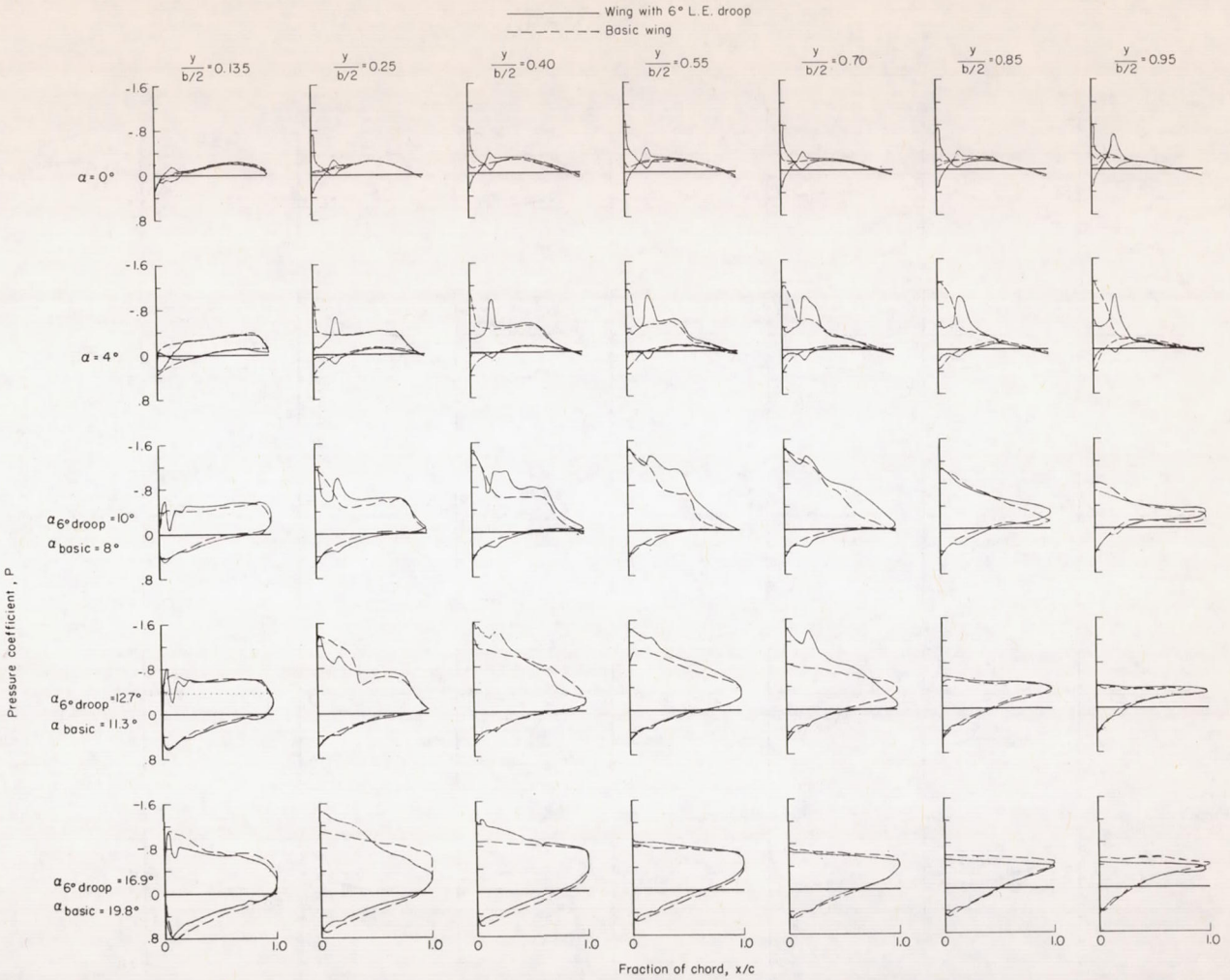


(b) M = 0.90.

Figure 3.- Continued.

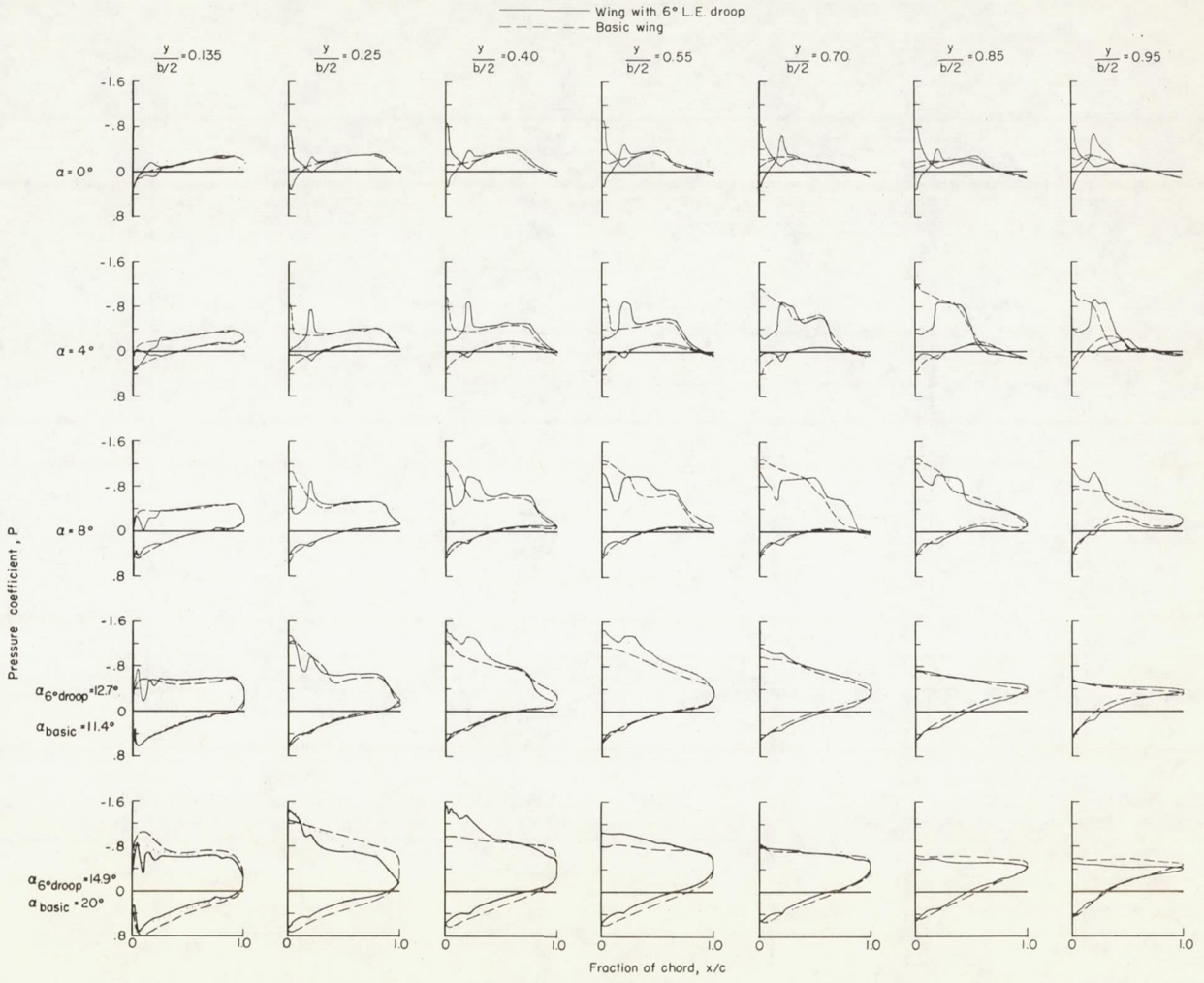


(c) M = 0.94.

Figure 3.- Continued.

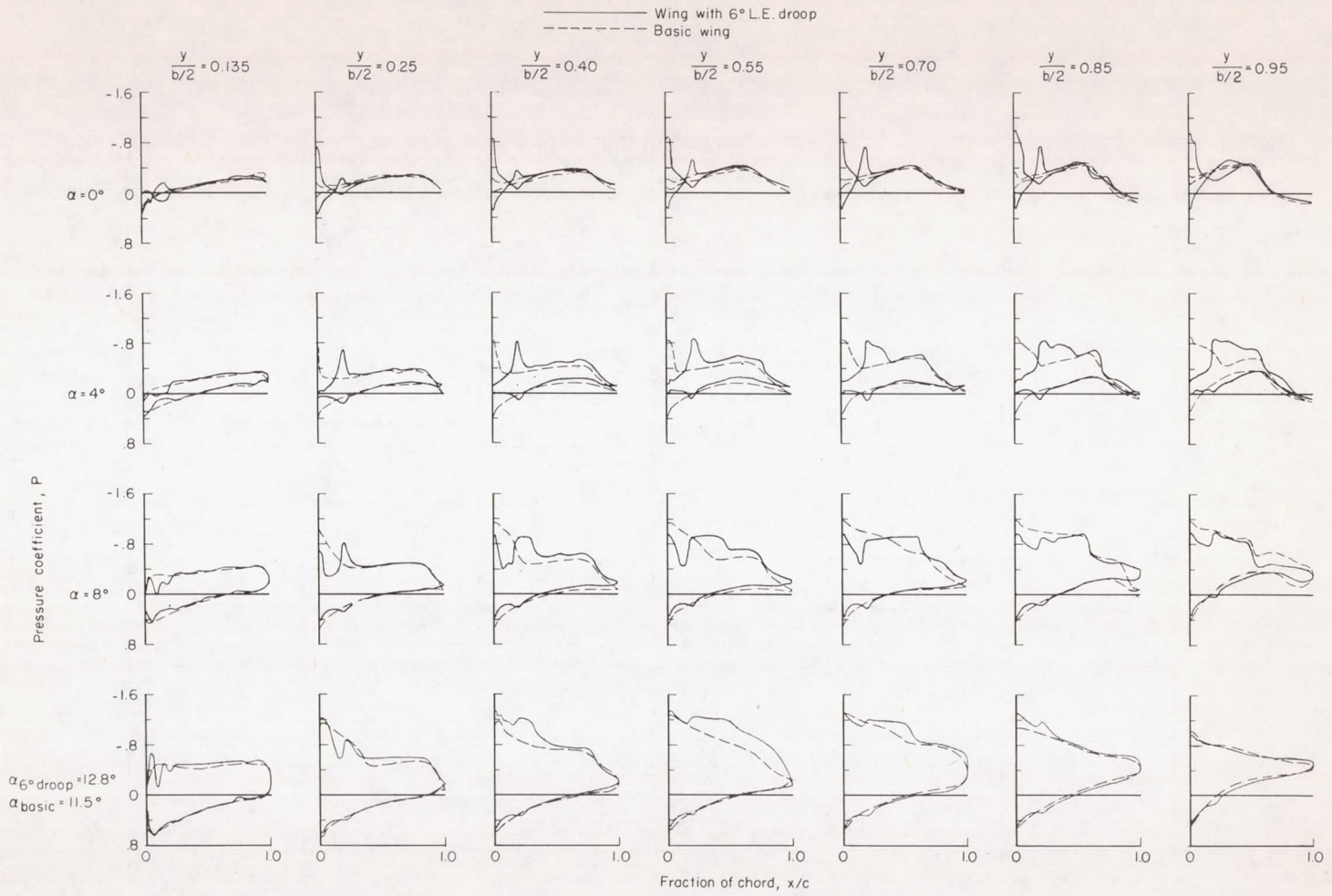


(d) M = 0.98.

Figure 3.- Continued.

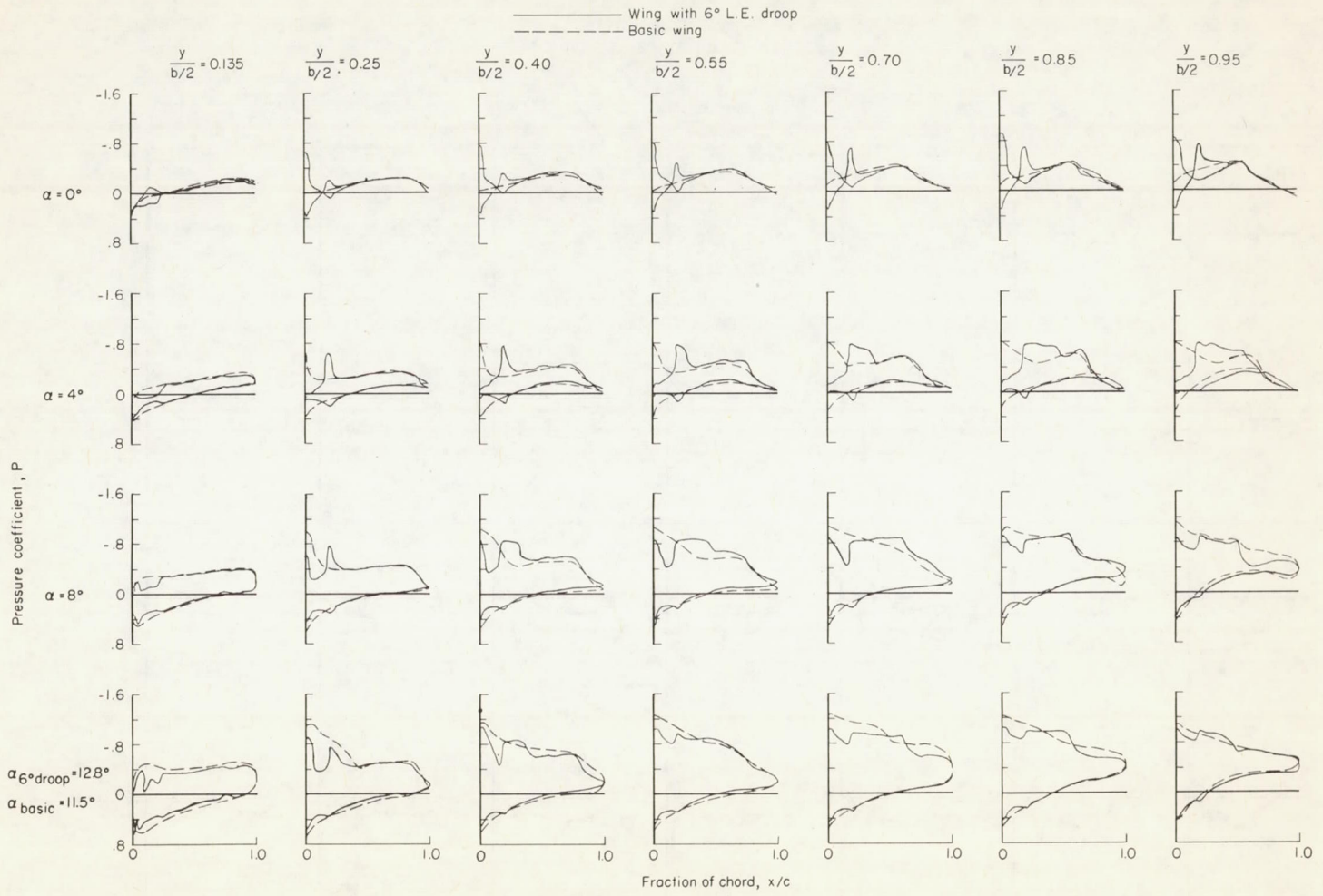


(e) M = 1.00.

Figure 3.- Continued.

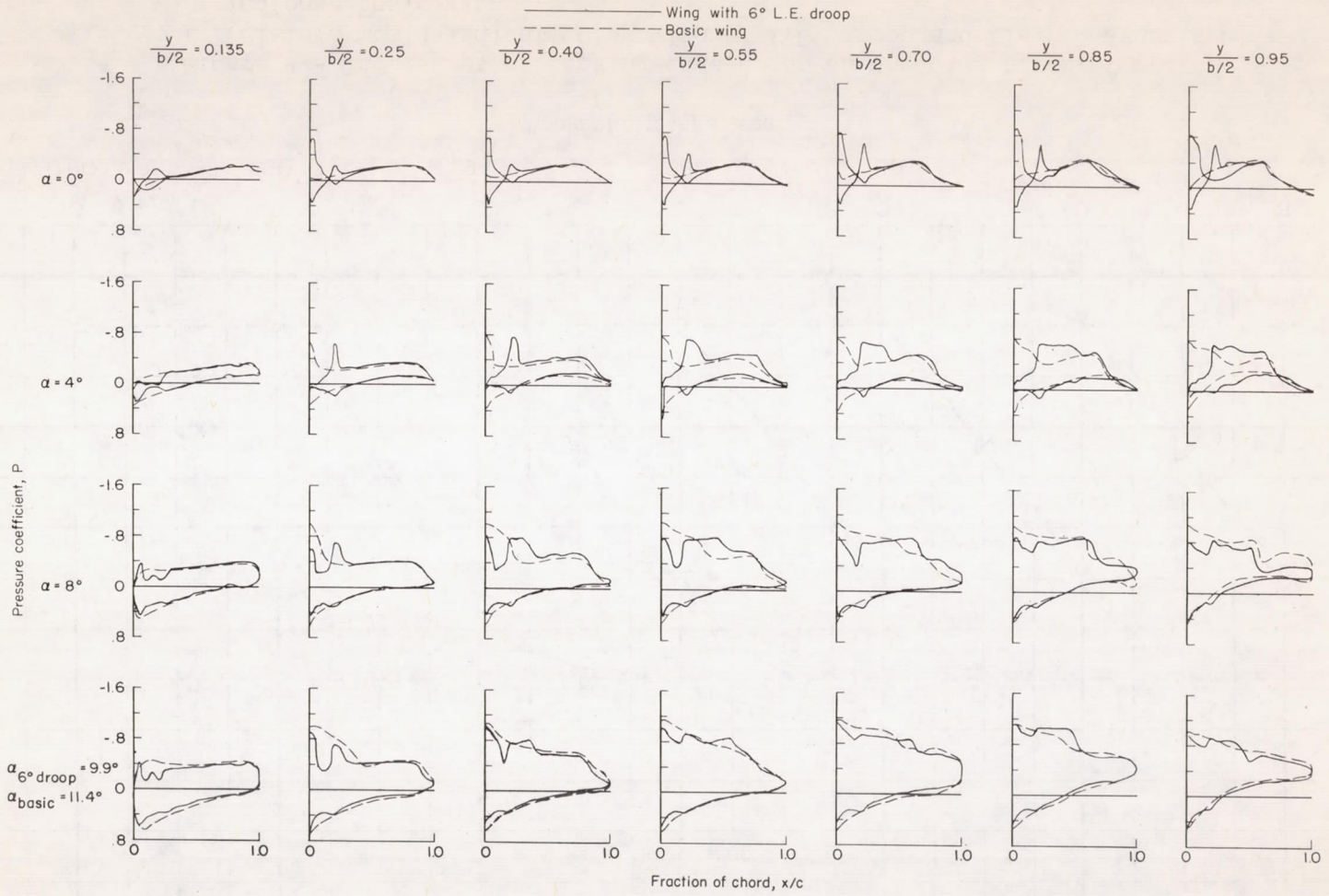


(f) M = 1.03.

Figure 3.- Concluded.

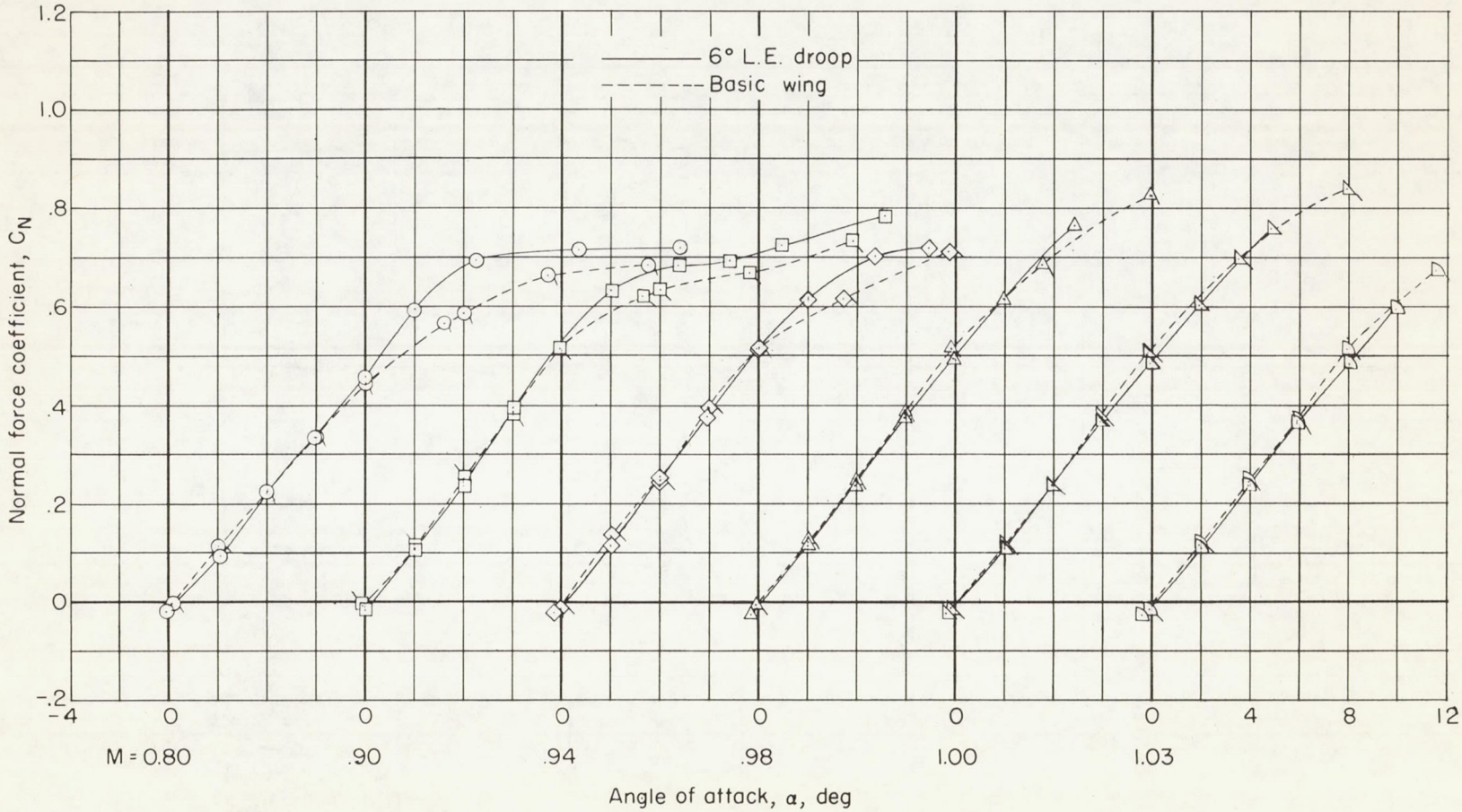


Figure 4.- The effect of leading-edge droop on the wing normal force. (Plain symbols indicate wing with 6° L.E. droop and flagged symbols indicate basic wing.)

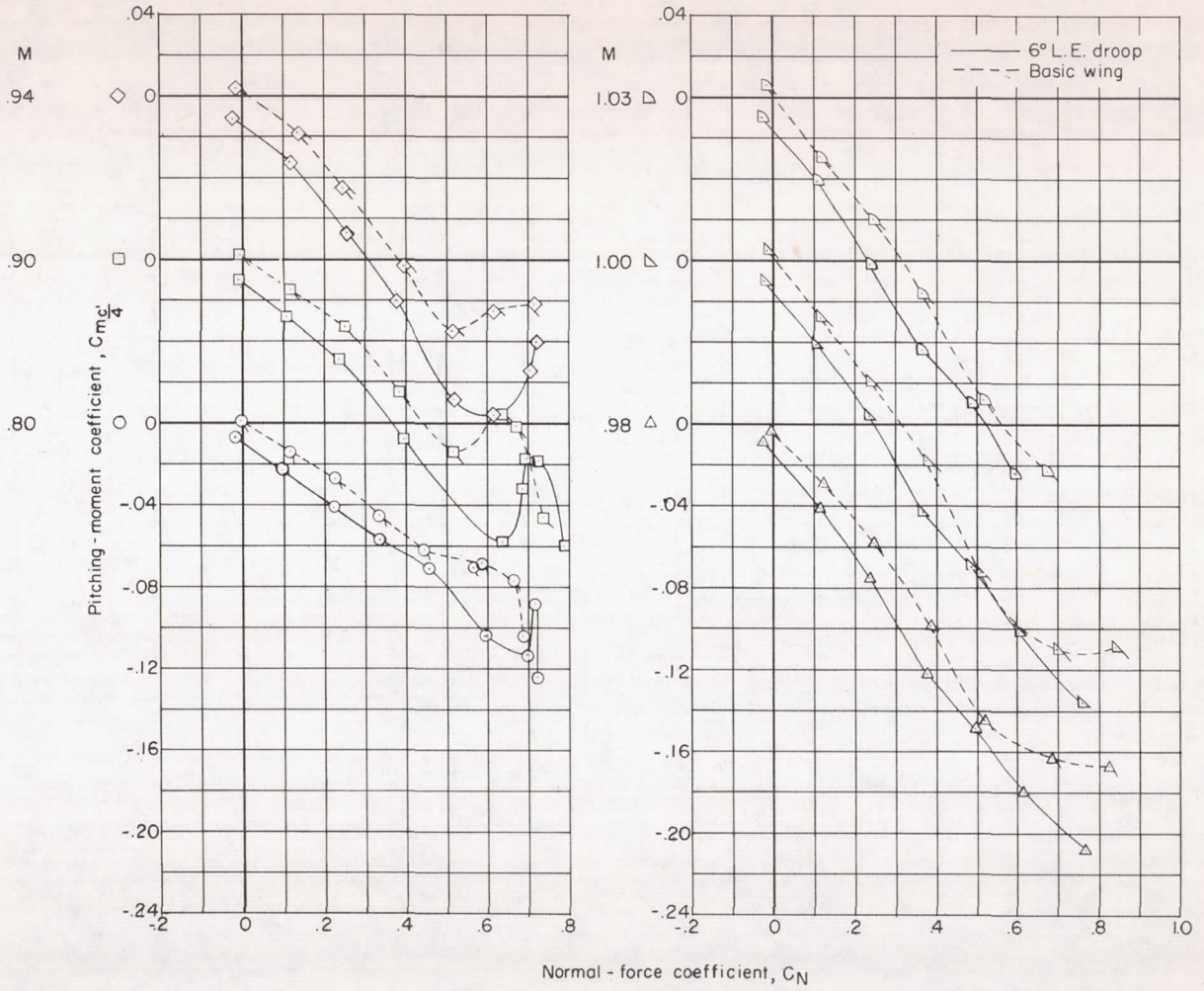


Figure 5.- The effect of leading-edge droop on the wing pitching moments. (Plain symbols indicate wing with L.E. droop and flagged symbols indicate basic wing.)

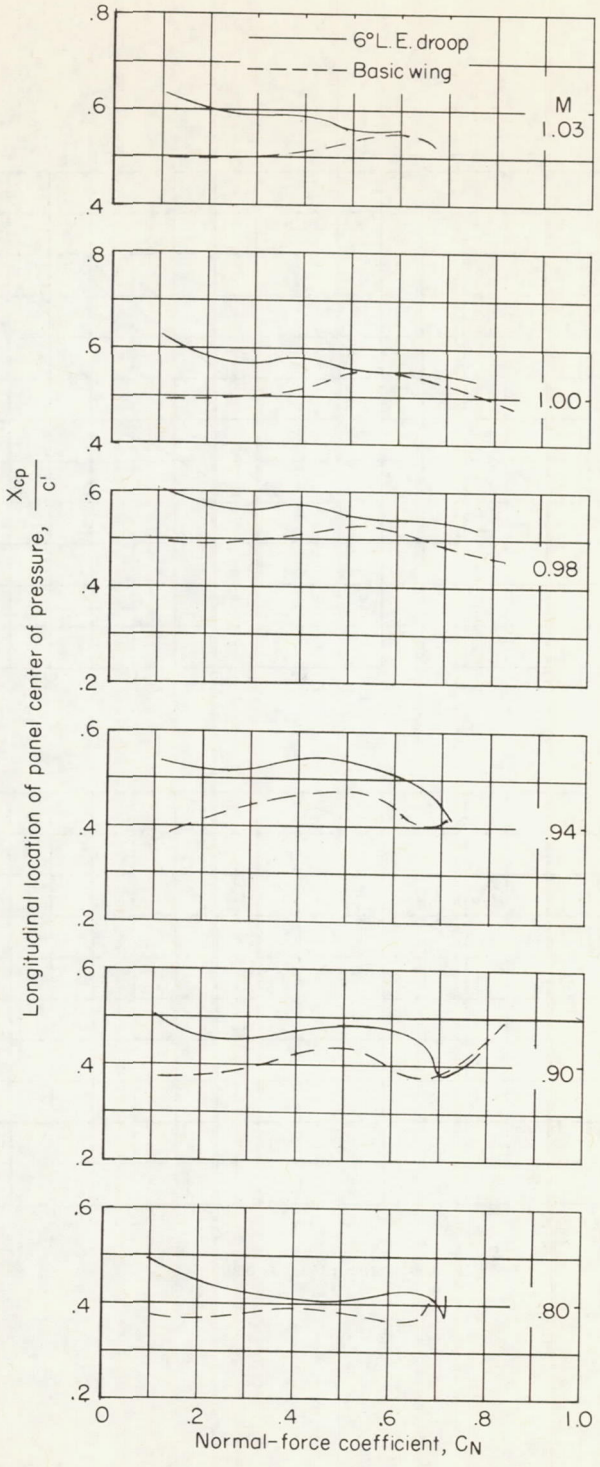


(a) Longitudinal.

Figure 6.- The effect of leading-edge droop on the wing center-of-pressure location.

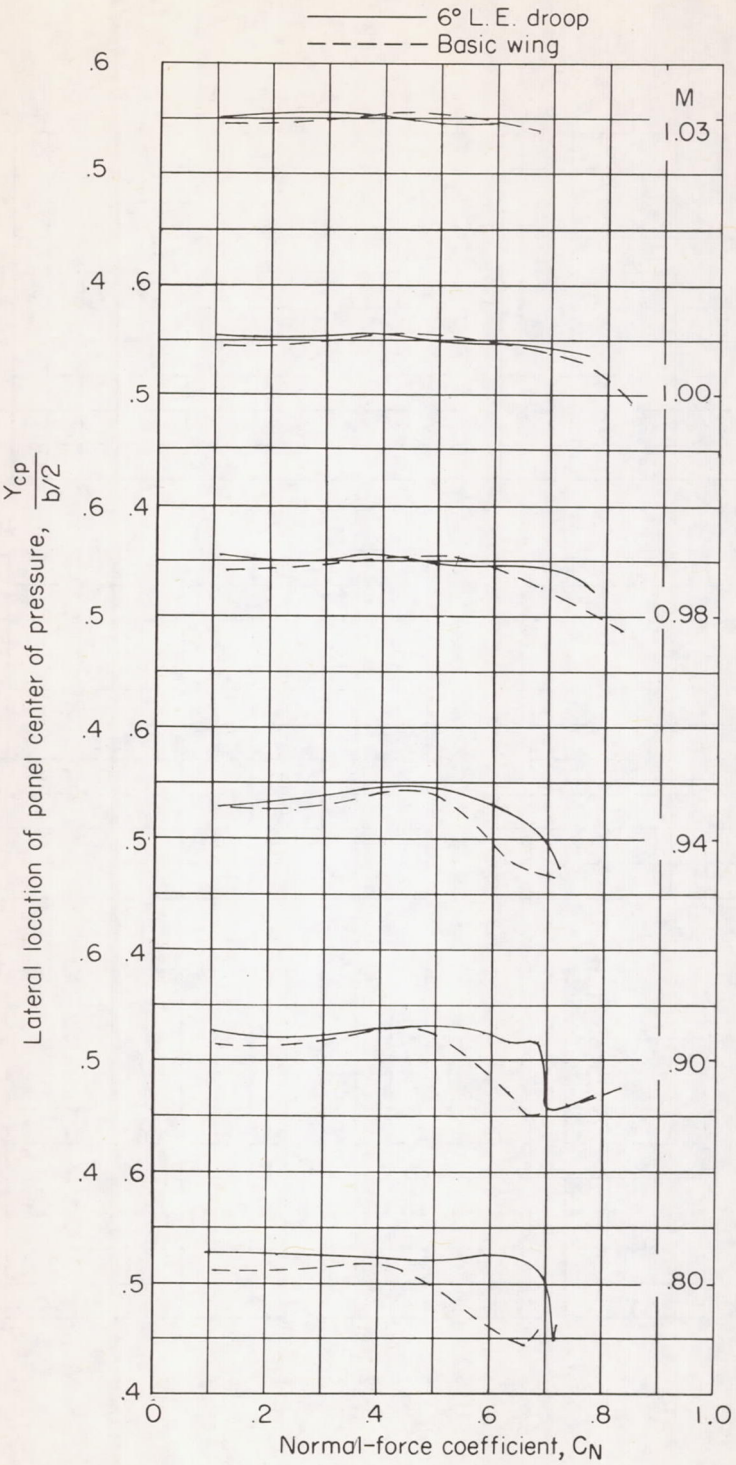


(b) Lateral.

Figure 6.- Concluded.

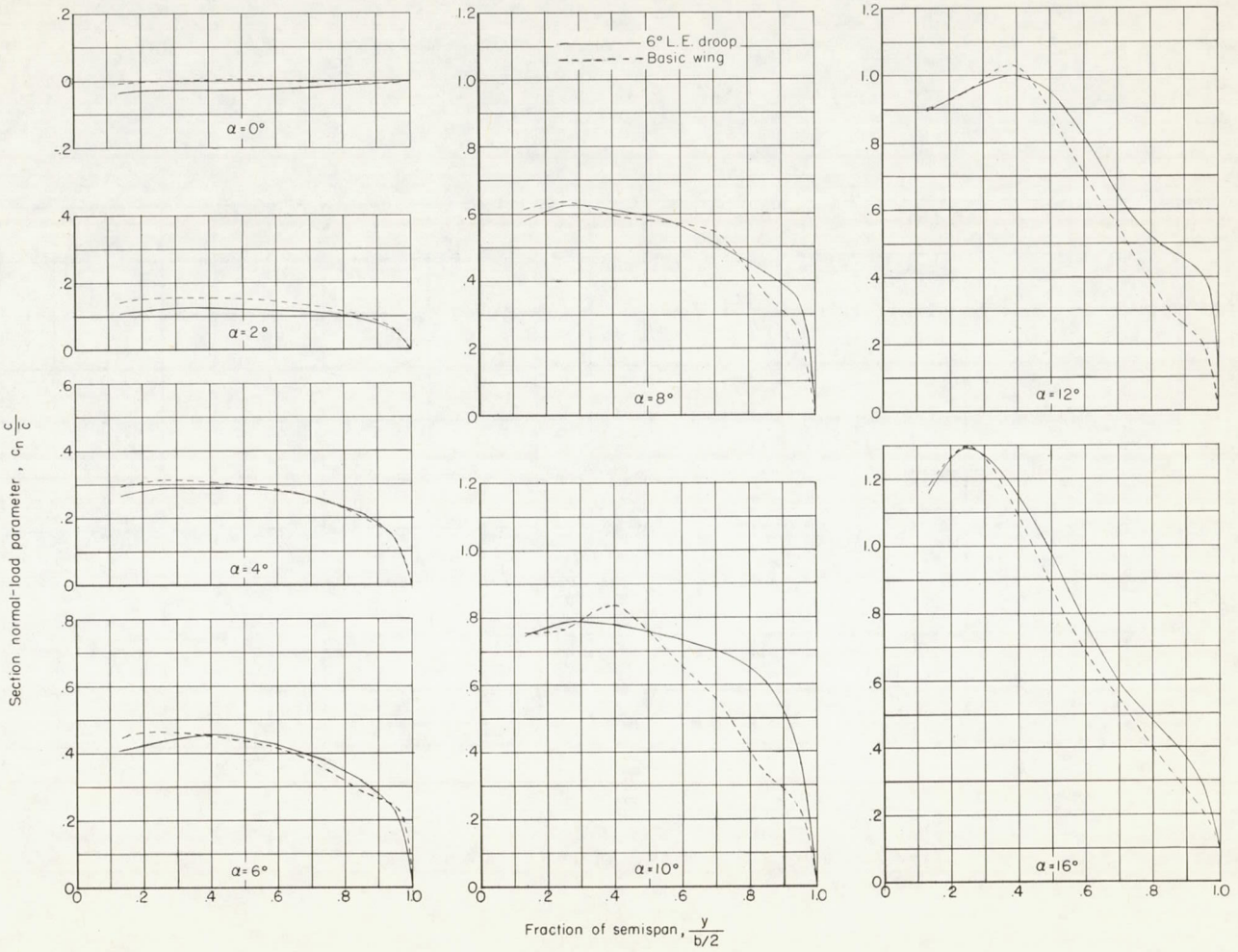


(a) M = 0.80.

Figure 7.- The effect of leading-edge droop on the wing semispan load distribution.

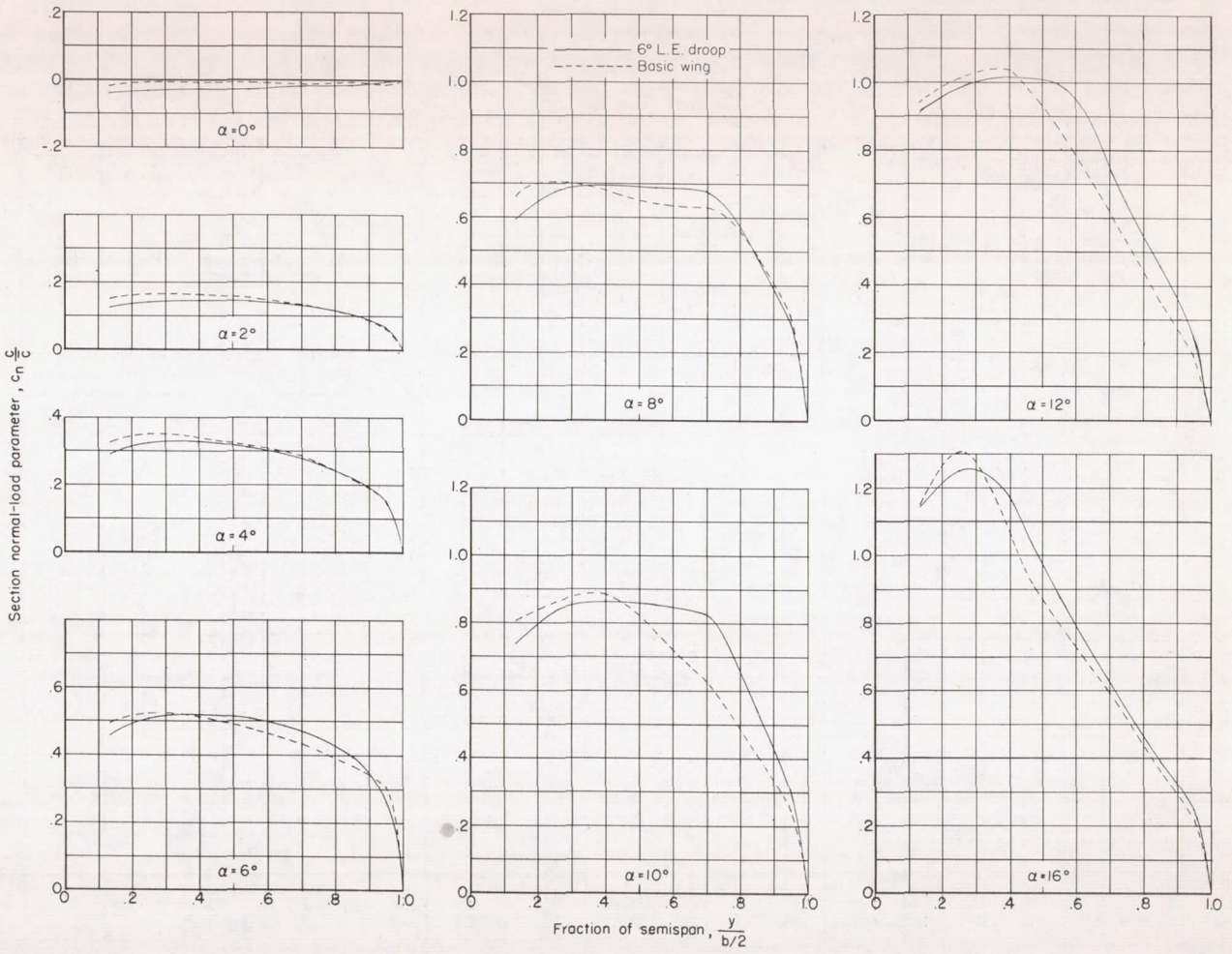


(b) M = 0.90.

Figure 7.- Continued.

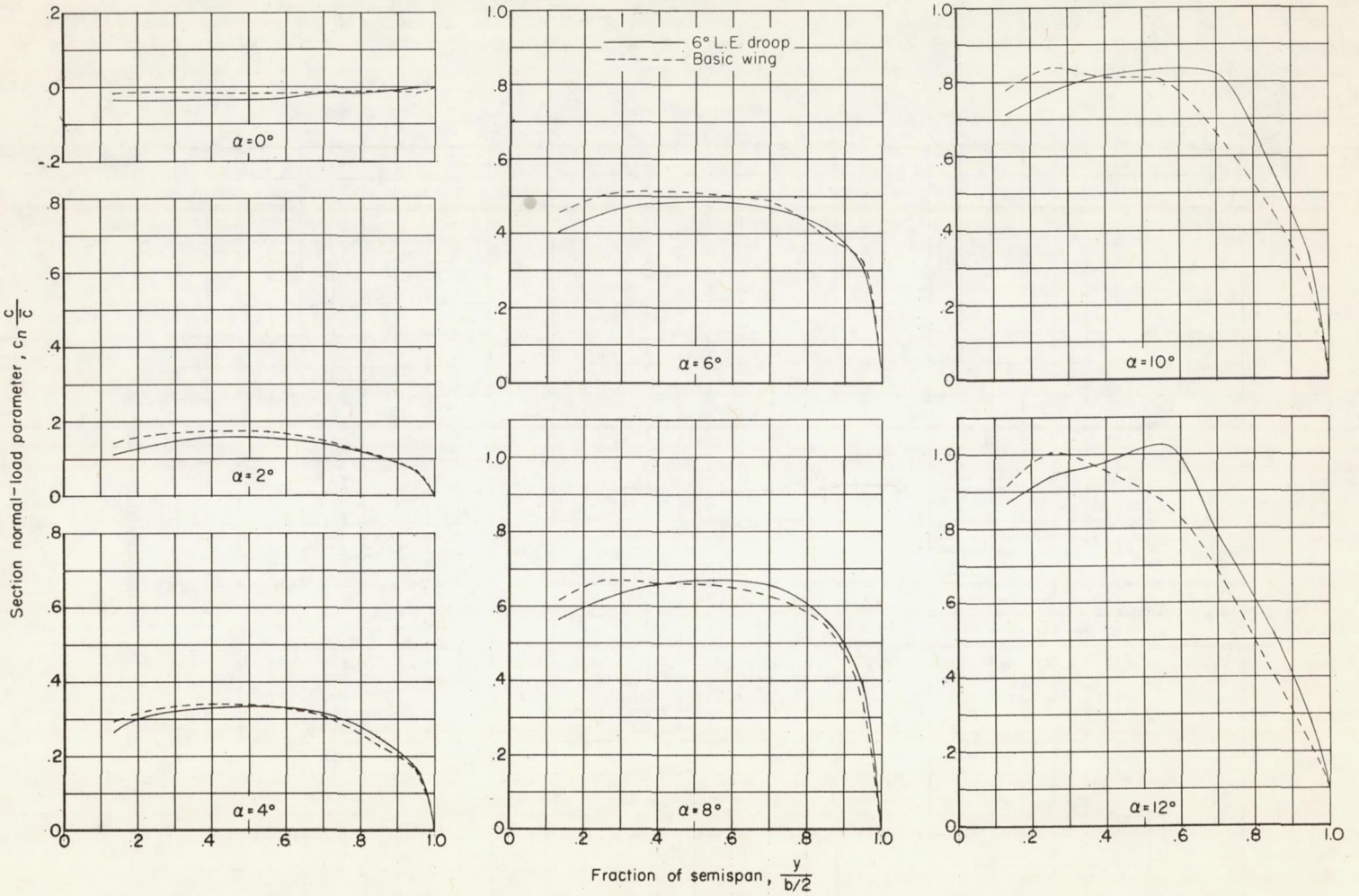


(c) M = 0.94.

Figure 7.- Continued.

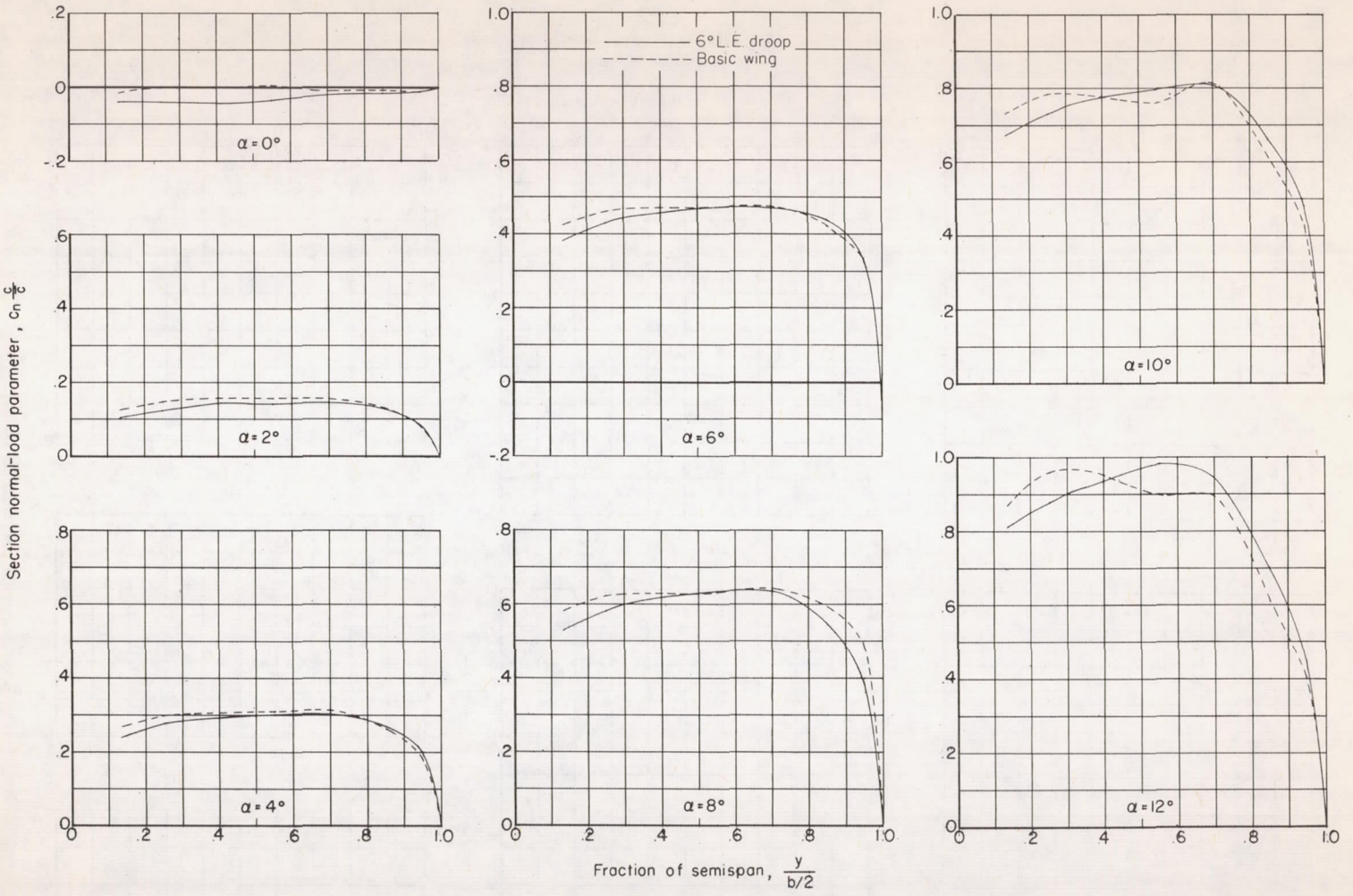


(d) M = 0.98.

Figure 7.- Continued.

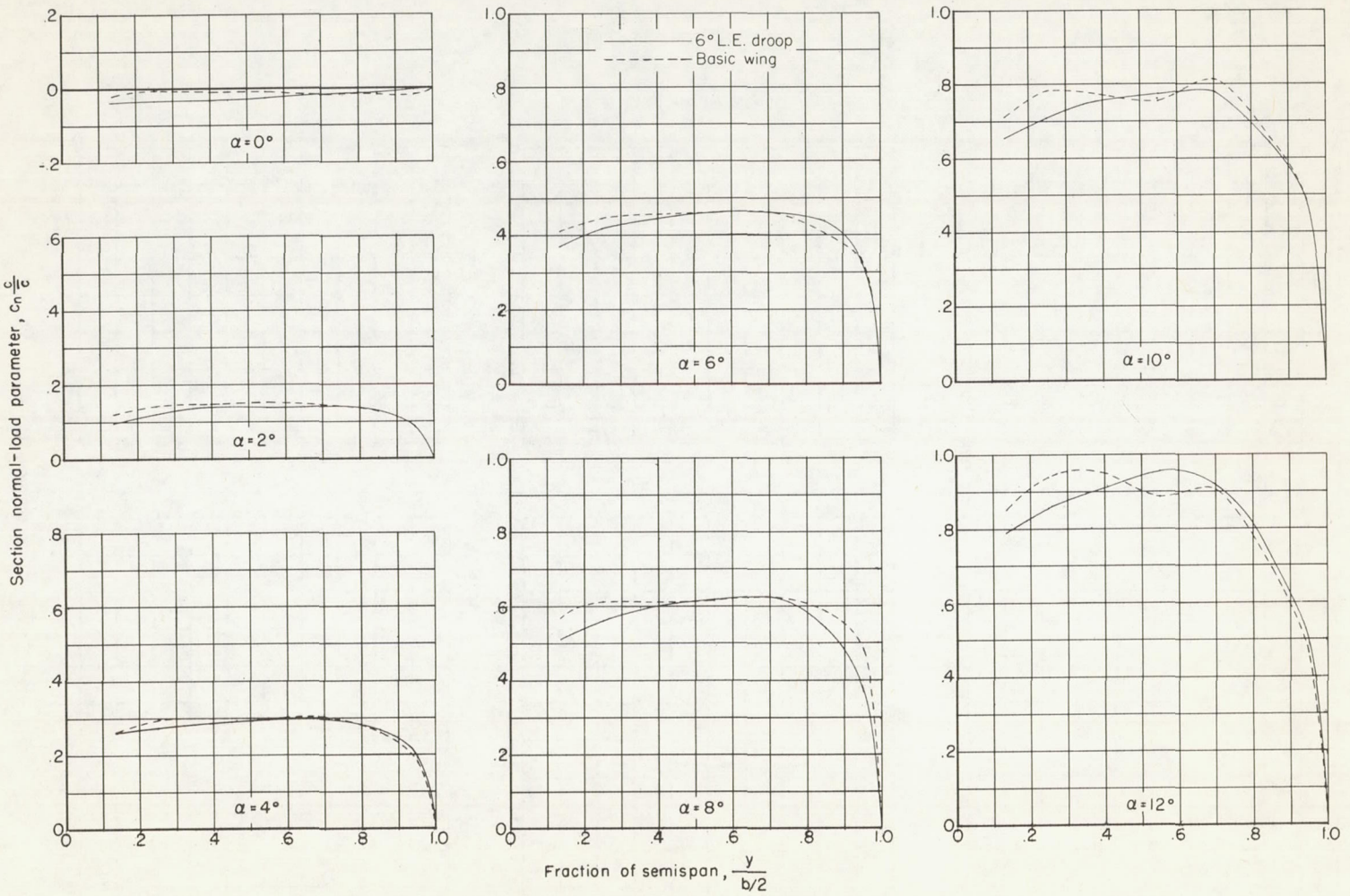


(e) M = 1.00.

Figure 7.- Continued.

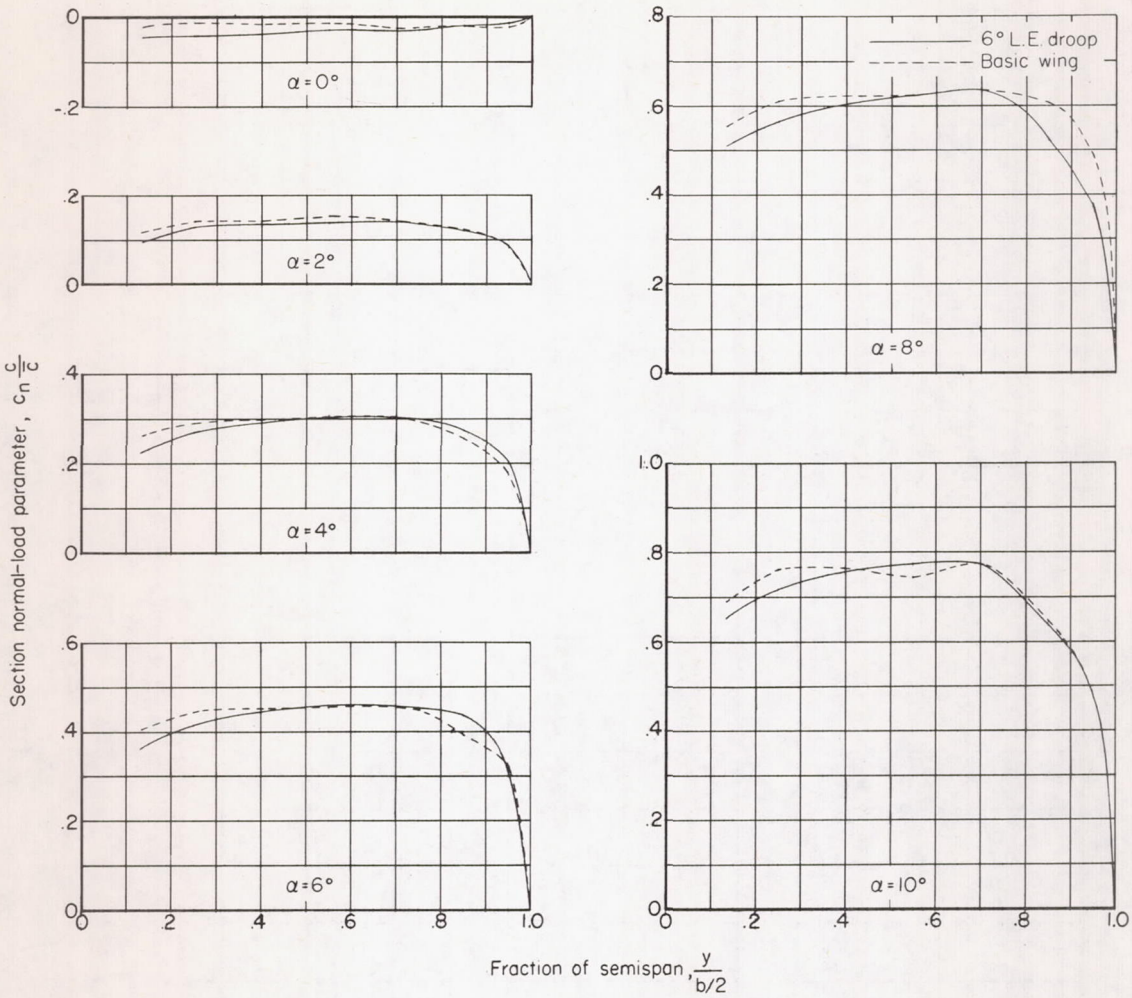


(f) M = 1.03.

Figure 7.- Concluded.

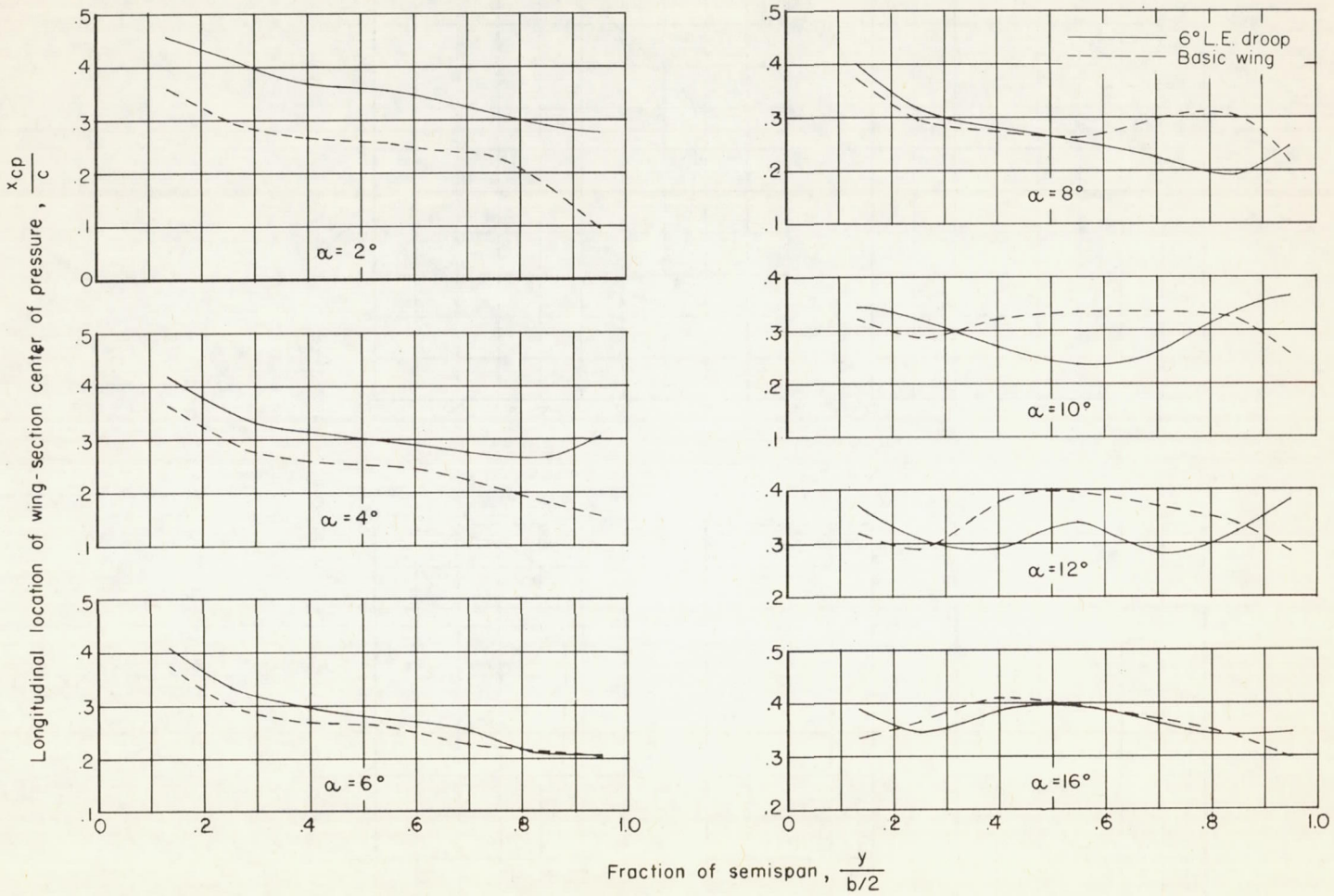


(a) M = 0.80.

Figure 8.- The effect of leading-edge droop on the longitudinal location of wing-section center of pressure.

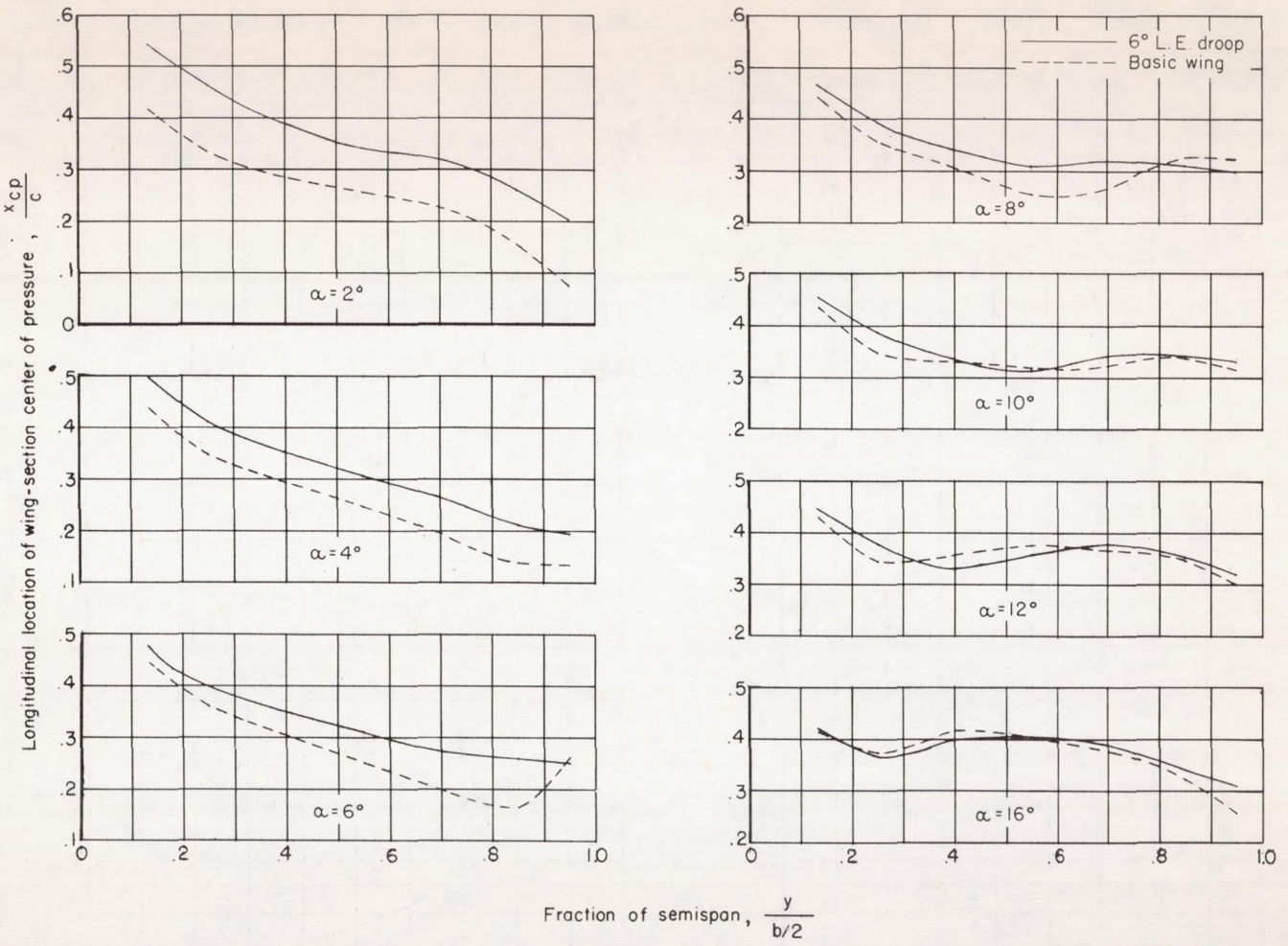


(b) M = 0.90.

Figure 8.- Continued.

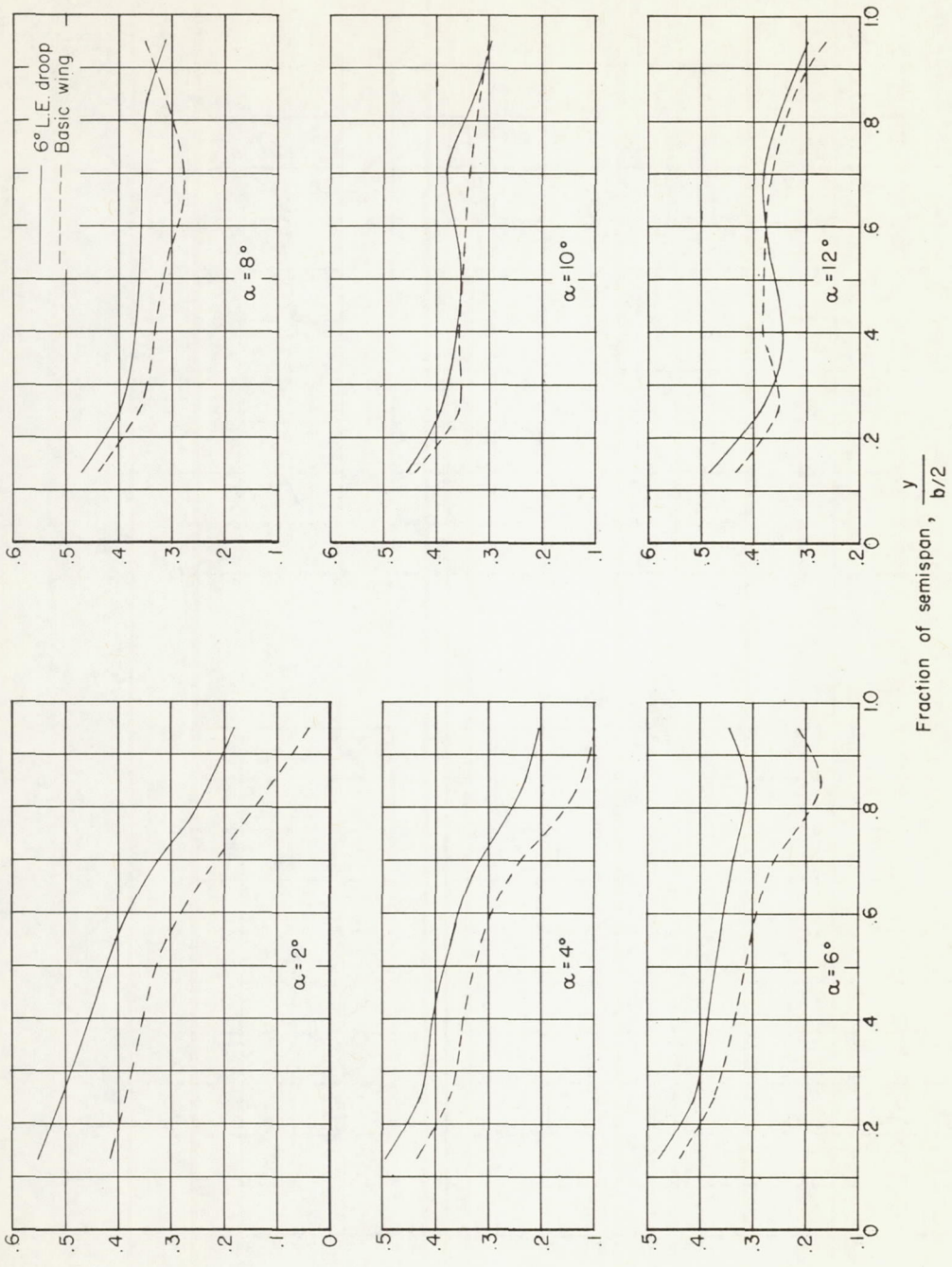


(c) M = 0.94.

Figure 8.- Continued.

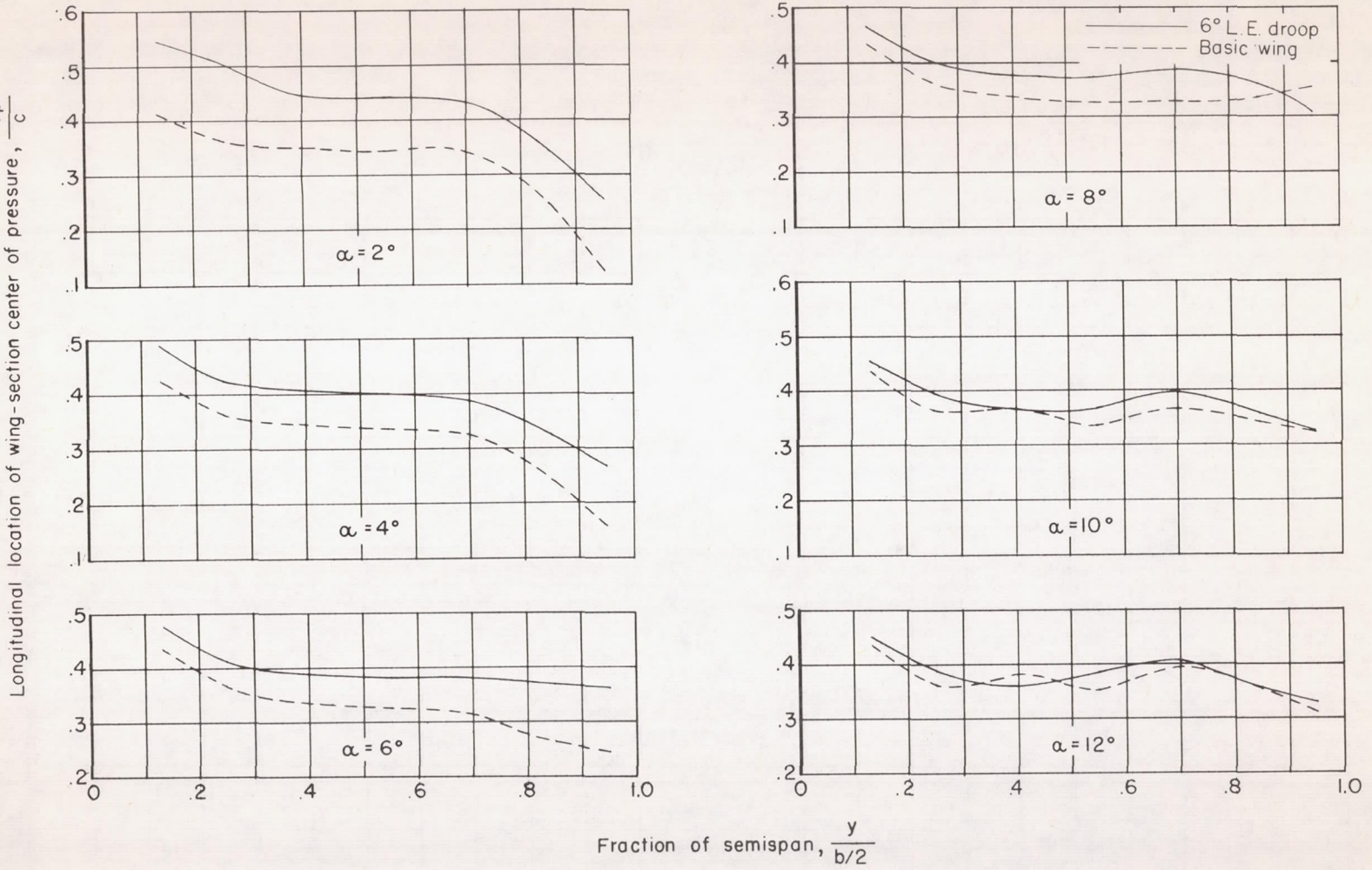


(d) M = 0.98.

Figure 8.- Continued.

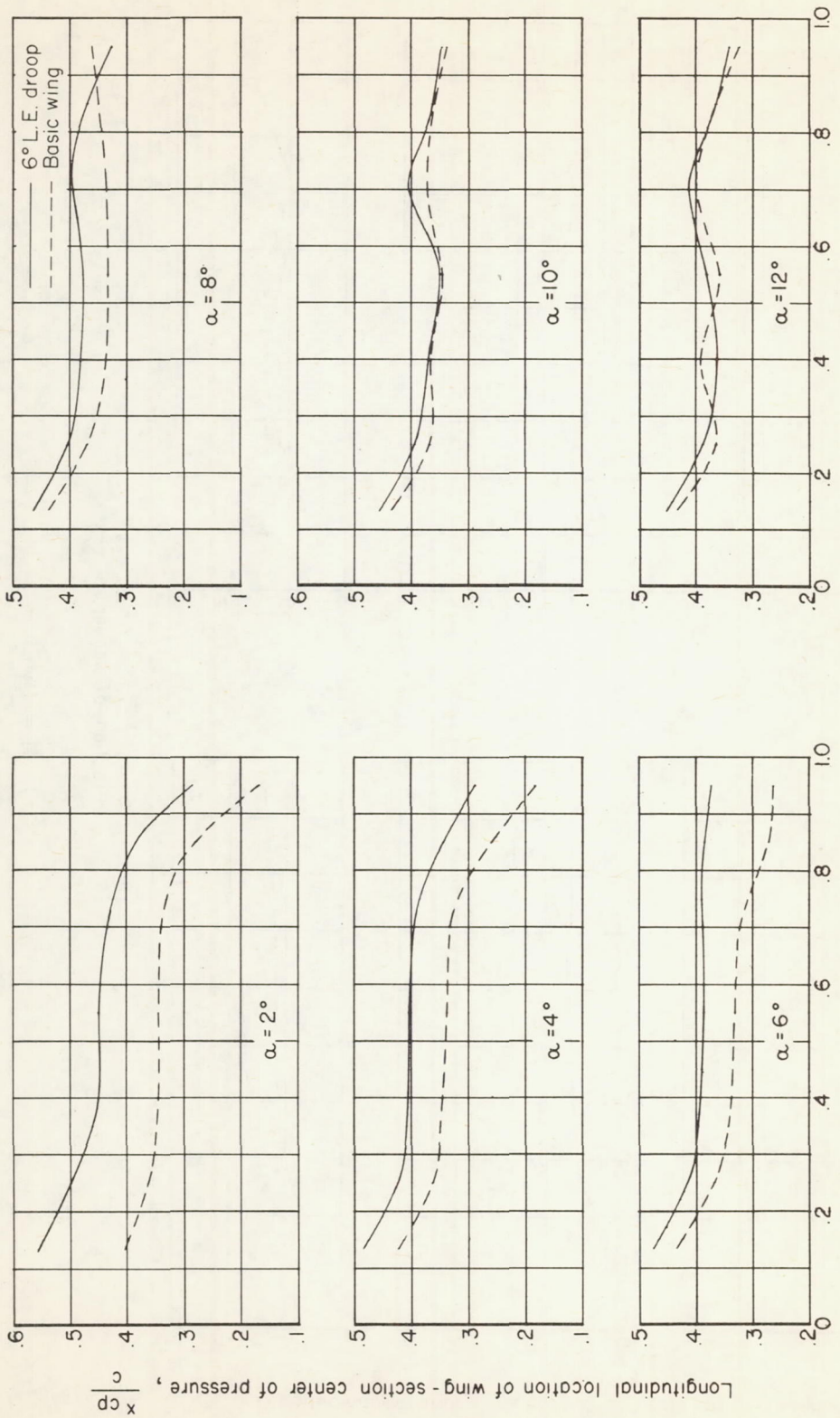


(e) M = 1.00.

Figure 8.- Continued.

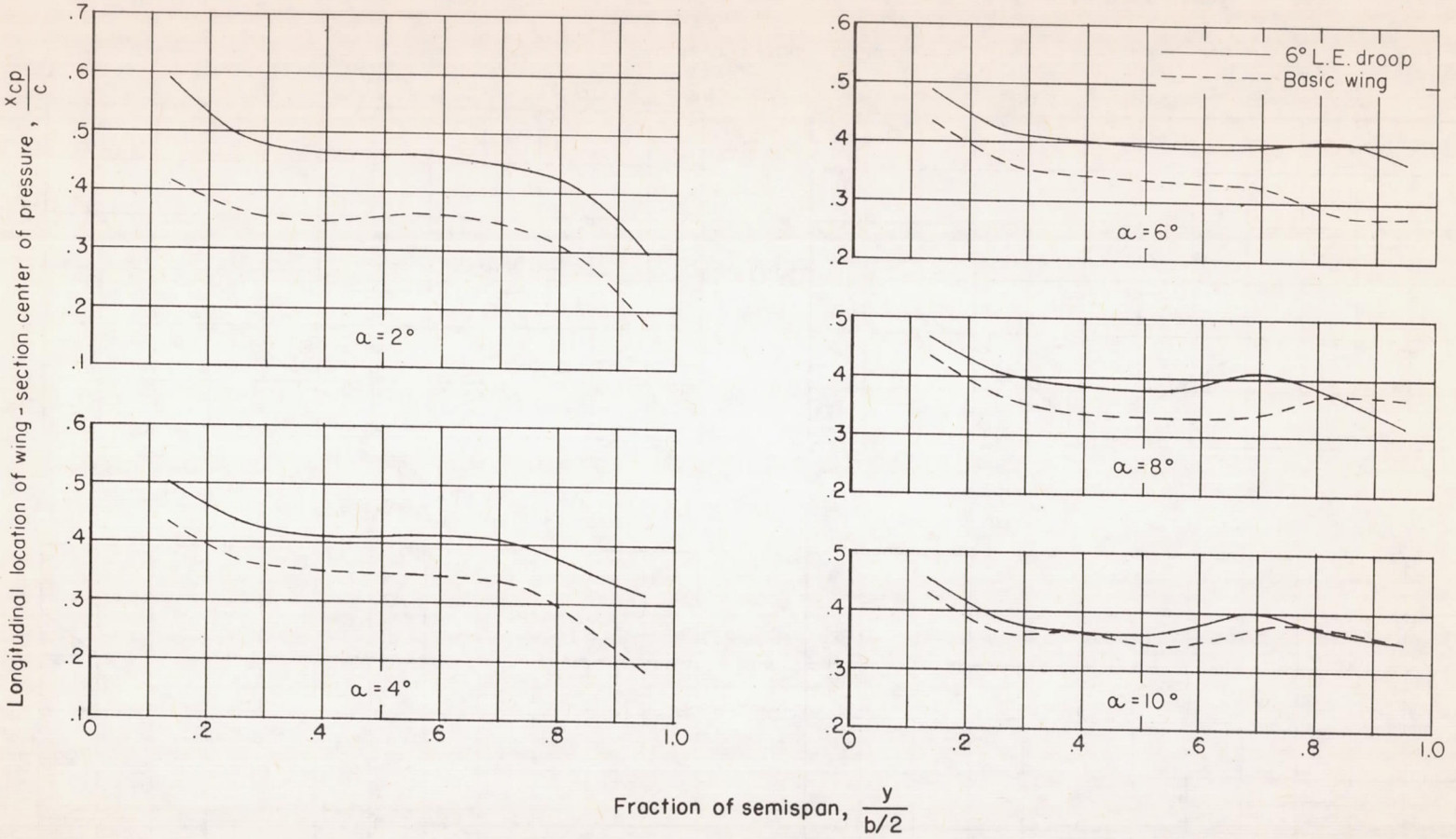


(f) M = 1.03.

Figure 8.- Concluded.

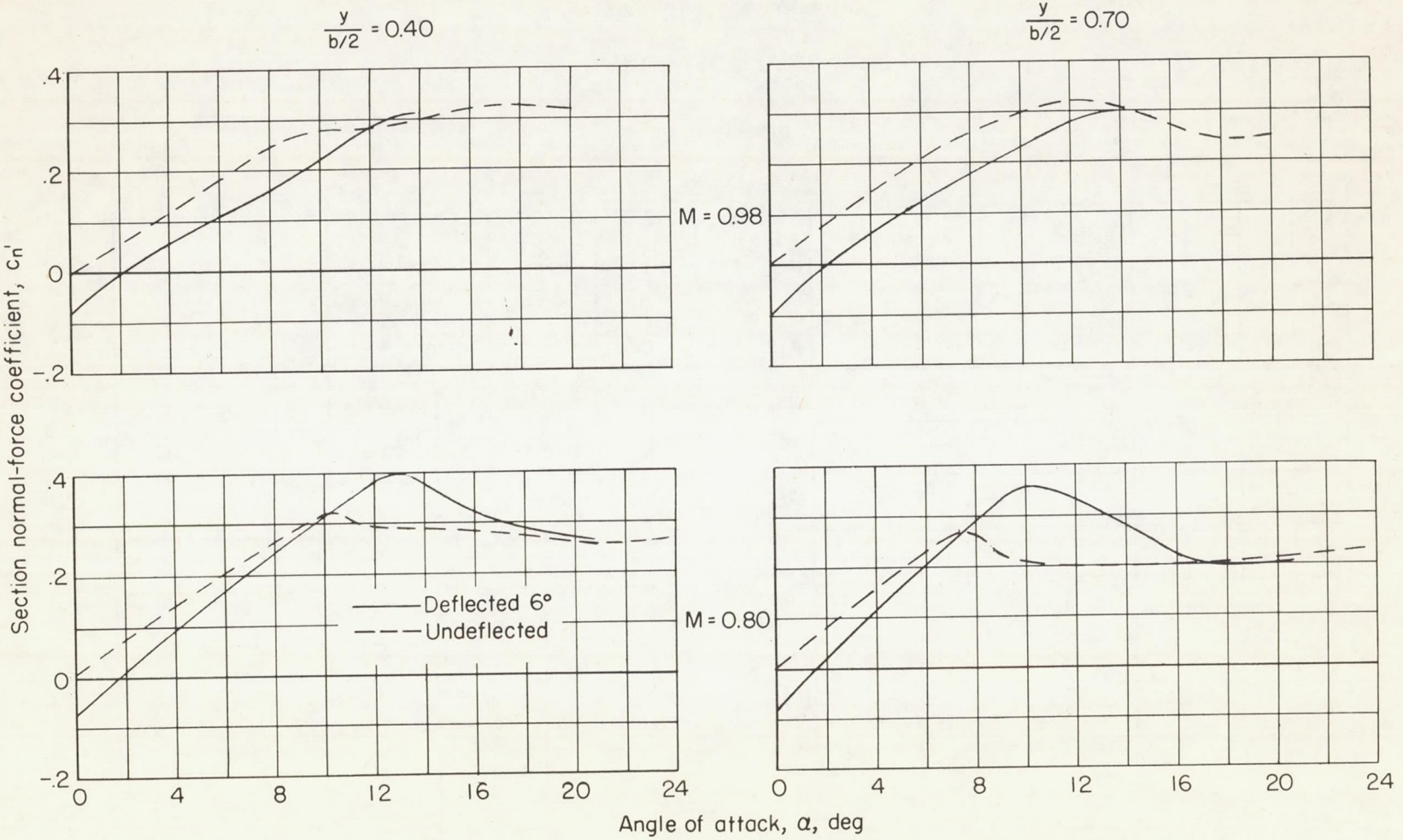


Figure 9.- Comparison of the normal-force coefficient for the forward 19 percent of the wing section deflected 6° and undeflected.

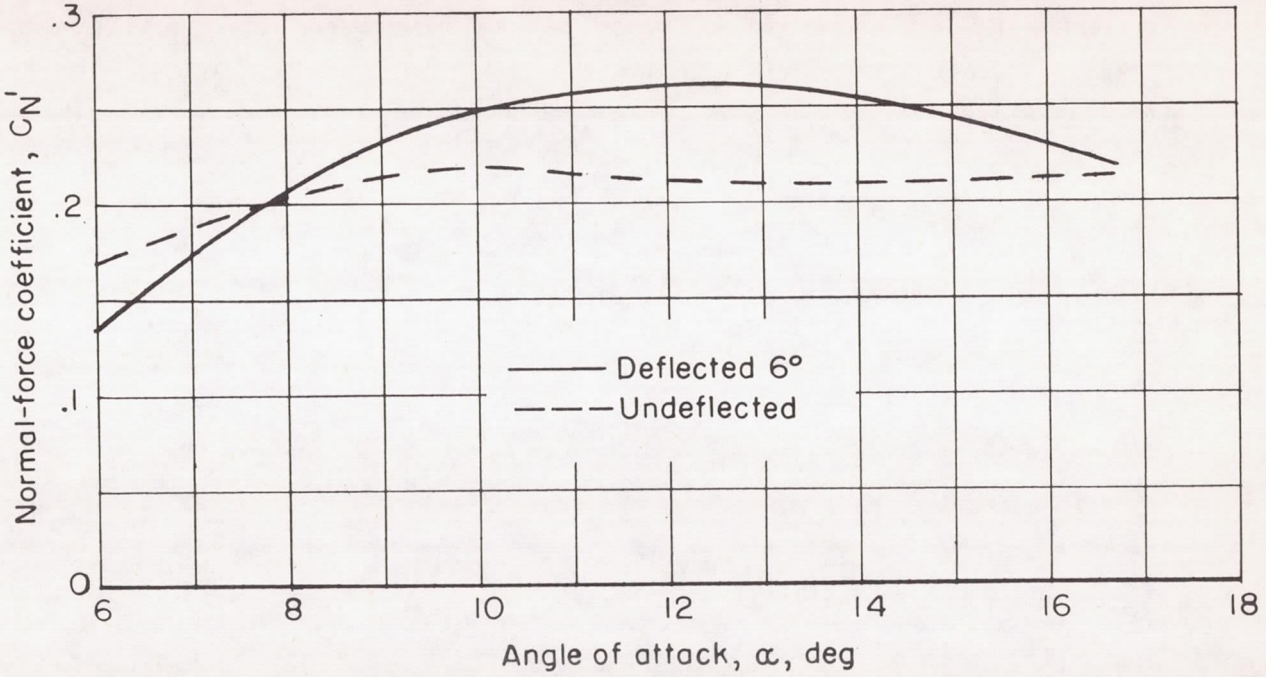


Figure 10.- Comparison of the normal-force coefficient for the forward 19 percent of the wing panel deflected 6° and undeflected. M = 0.80.

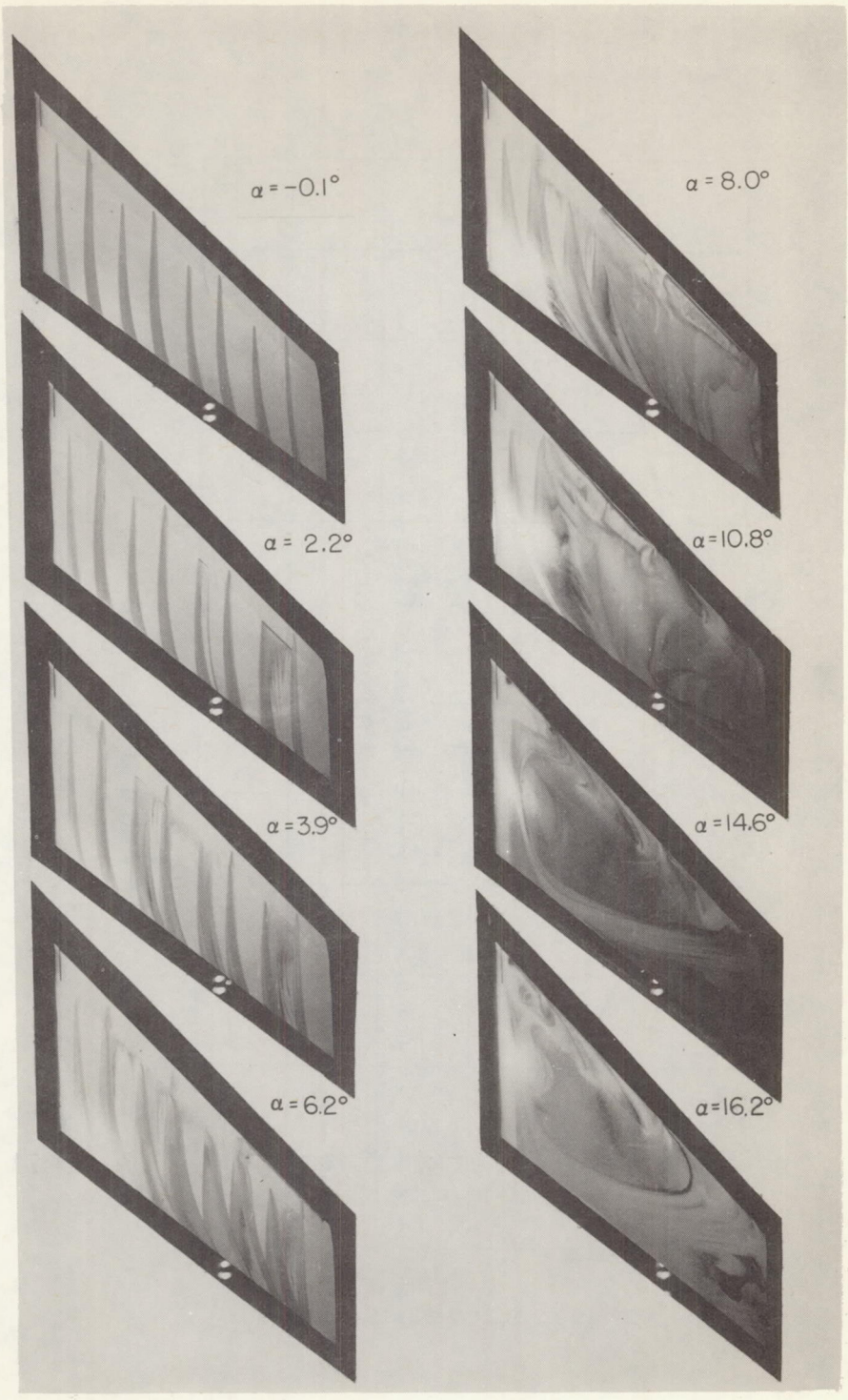


L-90483

(a) M = 0.80.

Figure 11.- Ink-flow pictures showing the flow over the upper surface of the wing with 6° leading-edge droop.

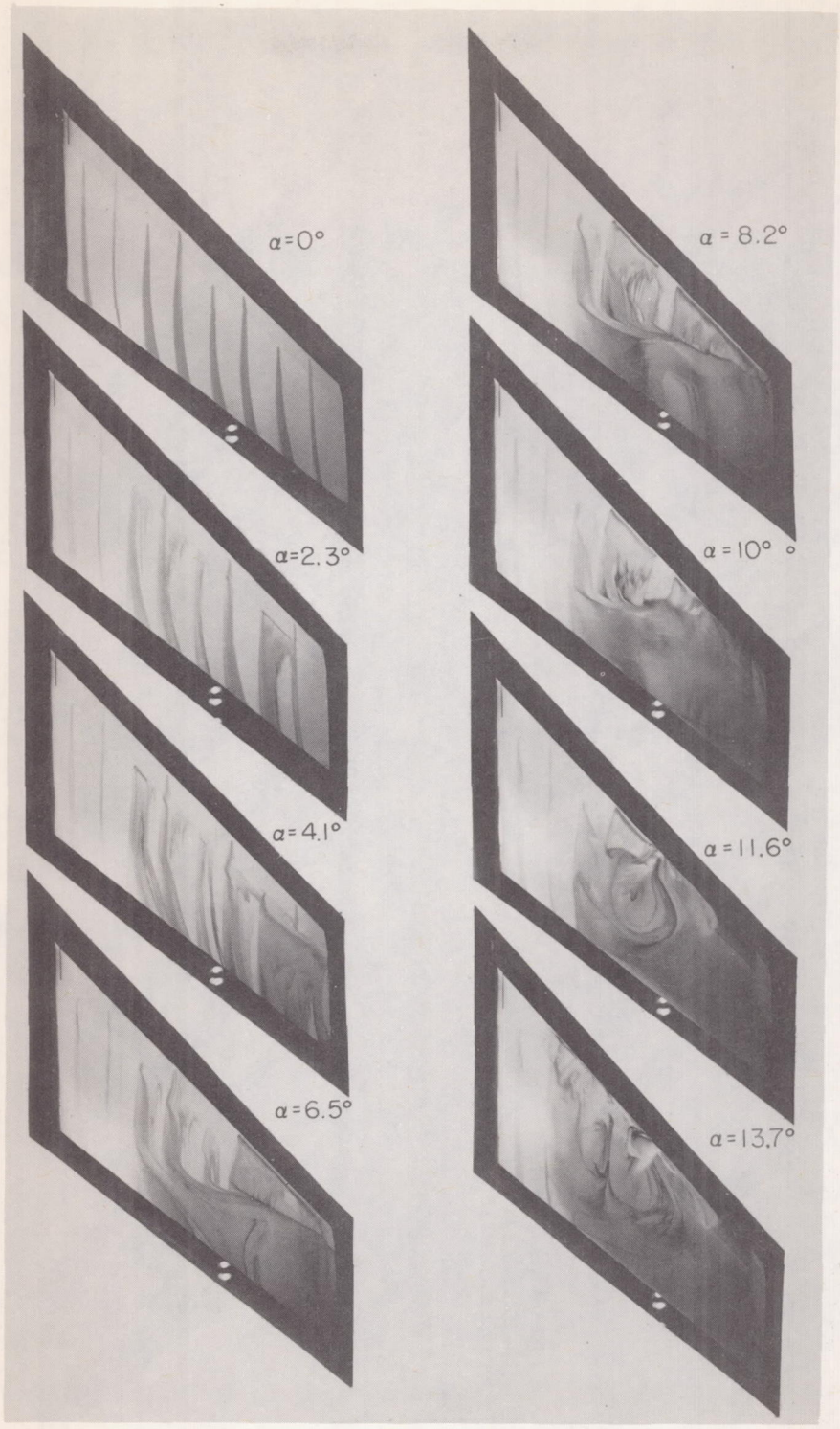


L-90484

(b) M = 0.90.

Figure 11.- Continued.

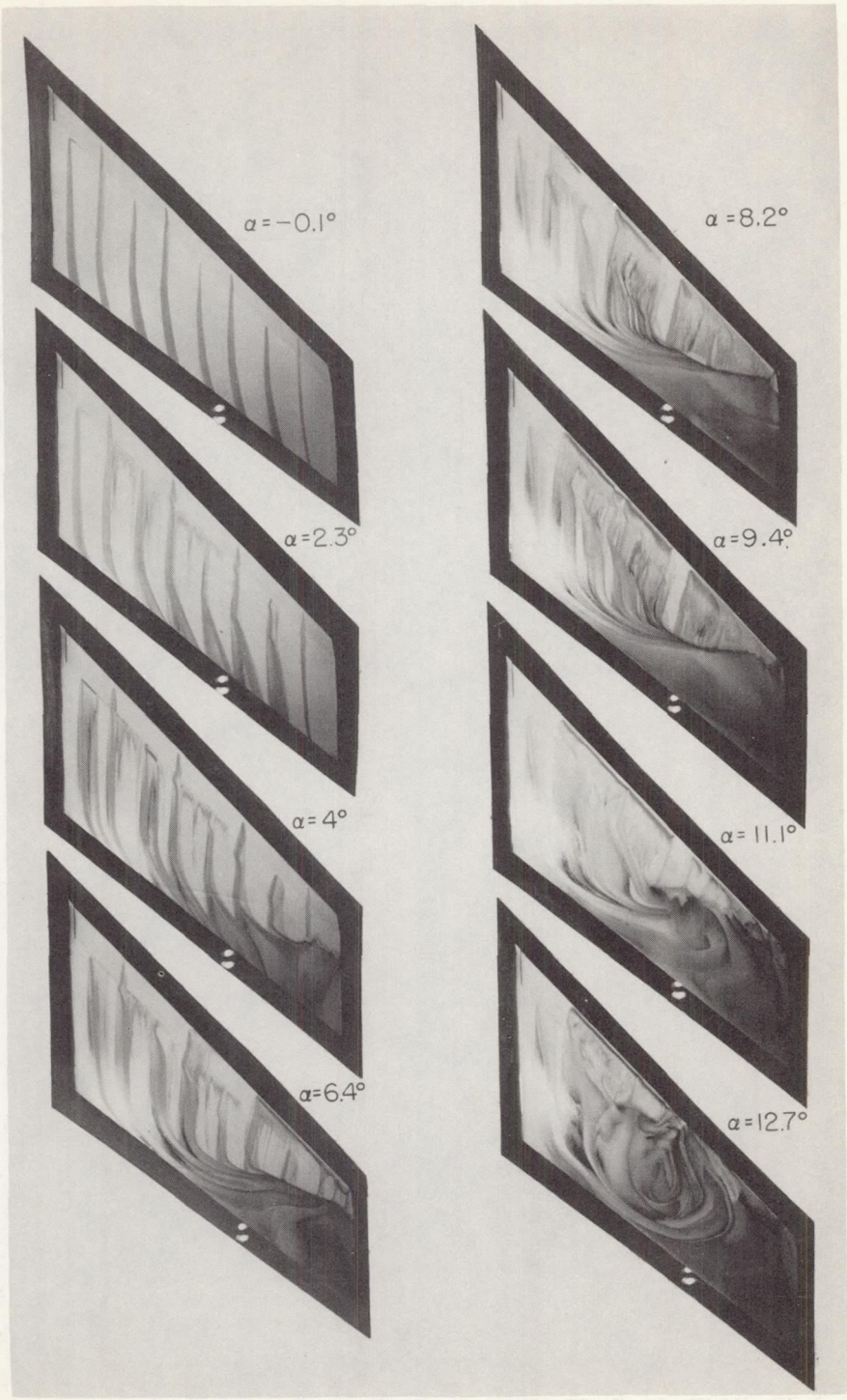


L-90485

(c) M = 0.94.

Figure 11.- Continued.

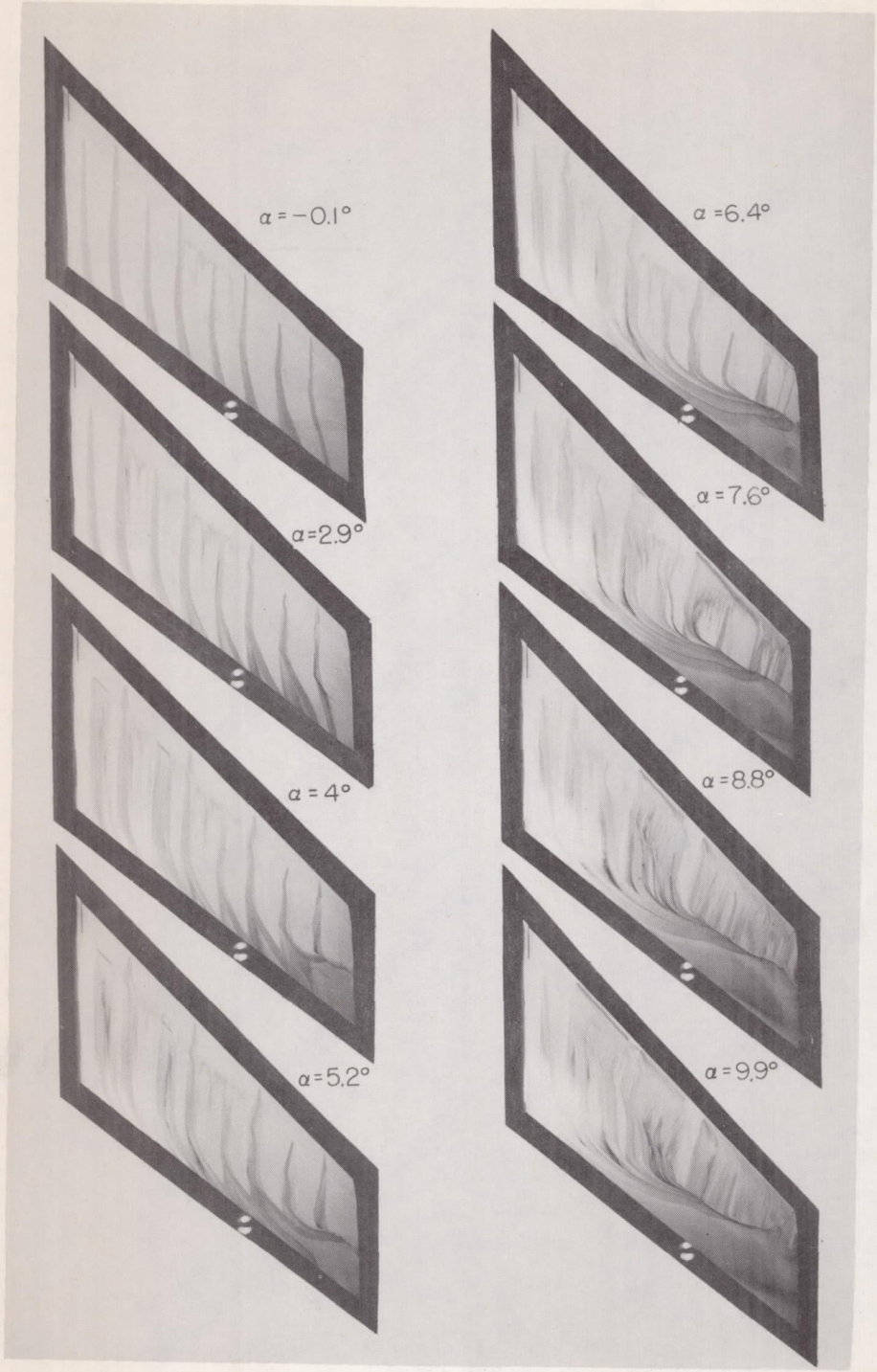


(d) M = 0.98.

L-90486

Figure 11.- Continued.

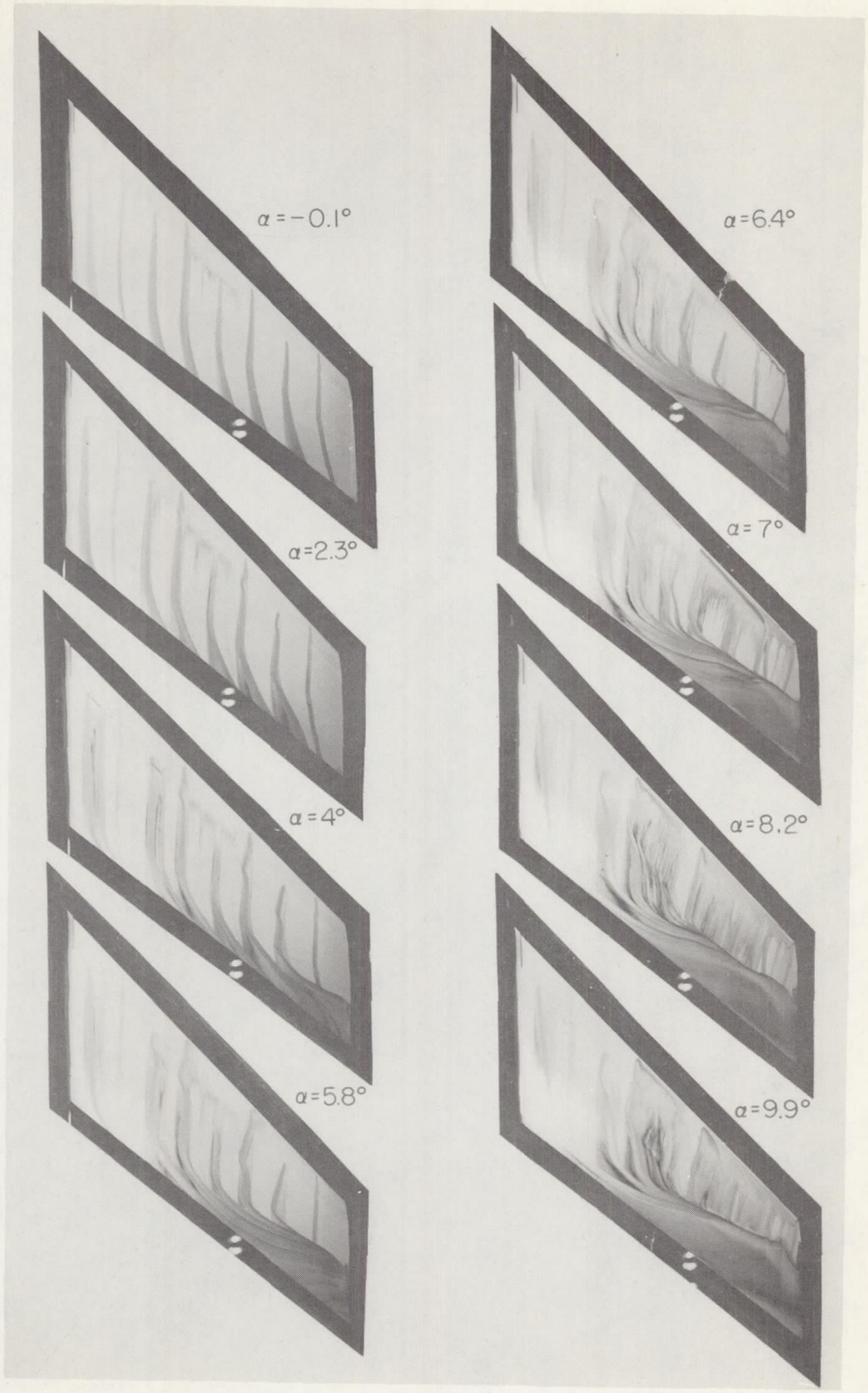


(e) M = 1.00.

L-90487

Figure 11.- Concluded.